THESIS

CHARACTERIZATION OF MIXED LINEAR ENERGY TRANSFER ENVIRONMENTS UTILIZING TISSUE-EQUIVALENT PROPORTIONAL COUNTERS

Submitted by

Joseph M. Fehrman

Department of Environmental and Radiological Health Sciences

In partial fulfillment of the requirements

For the Degree of Master of Science

Colorado State University

Fort Collins, Colorado

Summer 2023

Master's Committee:

Advisor: Alexander Brandl
Co-Advisor: Thomas Johnson

Kenneth Carlson

Copyright by Joseph M. Fehrman 2023

All Rights Reserved

ABSTRACT

CHARACTERIZATION OF MIXED LINEAR ENERGY TRANSFER ENVIRONMENTS UTILIZING TISSUE-EQUIVALENT PROPORTIONAL COUNTERS

There is currently great interest in the biological impact of radiological space exposures due to manned space missions (e.g., moon) where astronauts will face the challenge of living on board spacecraft for long periods of time. Cosmic radiation of many types exists in space and creates a unique mixed linear energy transfer (LET) environment. A tissue equivalent proportional counter (TEPC) was used to produce dose-equivalent measurements and quantify neutron exposures. Three neutron sources were used to simulate high energy, mixed LET environments: californium-252, a plutonium-beryllium source, and a deuterium-tritium neutron generator. TEPC dose-equivalent measurements can be utilized for basic research, and regulatory or clinical purposes for correlation with observable health effects. The main study was to quantify and compare TEPC dose equivalent rates in microdosimetric volumes to determine if significant dosimetric differences exist between mixed LET environments generated by photons and neutrons. The findings from this experiment showed that mixed LET environments where both photons and neutrons interacted with the TEPC had lower average LET values than neutron-only exposures, and produced varying dose equivalent rates that were dependent on the source characteristics. In summary, the TEPC was capable of monitoring in a mixed-LET environment and was successful at measuring the absorbed dose of high-energy photon and neutron interactions in space-like settings.

ACKNOWLEDGMENTS

I would like to thank my professors Dr. Alexander Brandl, Dr. Thomas Johnson, and Dr. Ralf Sudowe for their direction, mentorship, and support. The Radiological Health Sciences program would not be the same without them and the experiences they shared with us. I am thankful for Dr. Brandl and Dr. Johnson who made time in their busy schedules to assist me with all my questions and their support for this project. I also want to thank Dr. Kenneth Carlson, who took the time to be a part of my Graduate Committee. Additionally, I would like to thank Dave Oertli, Justin Bell, Paige Witter, Bal Parajuli, Noah Blair, Chrissy Falgren, Deb Thiele from Far West Technologies, and my peers for their support of my research and their contributions to making this project possible. All of my friends and colleagues made my time at Colorado State University fun and a memorable place for Abby and myself. I would also like to thank my loving family and friends for their continued support in my academic endeavors. I have spent a lot of time separated from them due to my work in the Air Force, but their love and support continue to push me to do more and help make my dreams come true. Thank you for always keeping in touch and making me feel loved. Lastly, I want to dedicate this paper to my wife, Abby Fenn, for allowing me the time needed to work on this project and as an excuse for getting out of doing chores around the house. Without Abby's love and support, I wouldn't have had the ability to write this thesis nor find the motivation to get this project done in a timely manner. This work was supported by the National Aeronautics and Space Administration (NASA) Specialized Center of Research on Carcinogenesis [grant number NNX15AK13G]. Disclaimer: The views expressed in this thesis are those of the author and do not reflect the official policy or position of the United States Air Force, Department of Defense or the United States Government.

TABLE OF CONTENTS

INTRODUCTION

Radiation Exposures in Space

The biological impact of high-energy neutrons represents a significant issue in space biology due to upcoming manned missions by several agencies across the globe, and the rapid development in commercial space exploration. High energy galactic cosmic and solar particle radiation interacts with the atmosphere and manned structures, such as the International Space Station, to produce secondary neutrons. Secondary neutrons have a very broad energy spectrum ranging from less than 1 to over 1,000 MeV (Kuhne, 2009). High-energy neutrons traveling at relativistic speeds interact with matter primarily through elastic and inelastic collisions with target nuclei. Neutron collisions result in interactions that produce secondary particles including charged particles (i.e., electrons), gamma rays, or recoil nuclei from neutrons produced in shielding and tissues. Both primary and secondary ionizing radiation are capable of penetrating through matter before transferring kinetic energy and eventually being absorbed. Severe localized damage may occur if the kinetic energy transfer results in a charged particle where the resultant Bragg Peak is in tissue mitochondria or DNA. Furthermore, acute exposures to high-energy, highly charged ions (HZE) are substantially more effective than gamma rays for the induction of solid tumors and deterministic effects in the human body.

Outside of low Earth orbit, astronauts will be exposed to high LET space radiation at a dose rate as high as 1.4 Gy per hour (NCRP 153, 2006). Unfortunately, there is little to no empirical data in any species regarding the carcinogenic effects of high LET or mixed LET radiation exposures at 1 mGy per day dose rates. The relative biological effectiveness (RBE) from neutrons is energy dependent and is optimal for neutrons around 1 MeV (BEIR VII, 2006). At very low doses, where there is an apparent increase in neutron RBE, reliable biological data is

difficult to obtain, especially for the reference low-LET radiation. Therefore, microdosimetric approaches are needed to evaluate the RBE for low doses of neutrons. Historically, RBE of neutrons has been determined from atomic bomb survivor data, from animal experiments using life expectancy, DNA damage, and mutations, *in vitro* cellular transformation rates, cancer mortality, and tissue-specific cancer incidences studies (Kuhne, 2009/NCRP 153, 2006). However, there is significant concern that the low dose rate of long-term exposures encountered in deep space may be more effective for tumor induction than acute exposures experienced by the atomic bomb survivors. Currently, NASA uses limiting conditions for radiation exposures of 3% cancer fatality risk to reduce the risk of cancer death due to exposures working in low-Earth orbit. Furthermore, additional limits are used to avoid clinically significant deterministic or non-cancer effects on the lens of the eye, skin, circulatory system, and central nervous system (Takahashi, 2018).

While progress has been made in understanding effects of radiation quality, far less is known about dose effects expected for extended missions beyond low earth orbit. Man-made sources of neutron-emitting radiation are commonly employed as substitutes for the high LET radiation encountered in space. Utilizing the ^{252}Cf source, PuBe source, and the DT generator offers a significant advantage as they encompass a comprehensive range of energy spectra from man-made sources with varying average LET. It is this average LET that we aim to replicate as a substitute for the exposure of astronauts to HZE particles. Therefore, these three sources represent the sole options for generating average LETs within a laboratory setting, except for accelerator experiments, which have been limited in running at low dose rates for extended durations. Neutrons in space have a wide range of energies, and understanding their energy distribution is critical for comprehending their impact on human tissue. The charged particle

nuclei generated by these fast neutron interactions in tissue have dose-response curves, LET distributions, and RBE similar to HZE ions (Borak, 2019). This study is designed to characterize the mixed LET from photon and neutron interactions within a TEPC to measure and define the absorbed dose and dose-equivalent for human tissue at micro-simulated volumes. The main goal of this study is to demonstrate that the TEPC generates reliable data concerning absorbed dose and dose equivalent rates across a range of neutron spectra originating from three man-made neutron sources, including low LET contributions.

Tissue-Equivalent Proportional Counters (TEPC)

In the past, NASA integrated the use of tissue-equivalent proportional counters within the International Space Station and space shuttles for the purpose of monitoring the radiation field inside the spacecraft (Gersey, 2006). Proportional counters used in this study are based on a spherical Rossi Chamber that employs a spherical chamber with tissue equivalent (TE) walls and TE fill gas. The TE walls are made of Shonka Type-A (A-150) plastic that has similar tissue density to that of human tissue. The TE fill gas consists of propane gas (C_3H_8) filled at a low pressure that can be adjusted to simulate the volume of a human cell. The average human cell size ranges from 3 to 120 μm wide (Barth, 2017). The purpose of the TEPC is to measure the lineal energy and absorbed dose of radiation energy deposited within small volumes similar to human tissue. The detector has a spherical shape to keep the response independent of the direction of the incident radiation. A fine helical wire surrounds the anode wire to prevent distortion of the electric field where the anode meets the cathode wall instead of having a singular anode wire running along the diameter of the sphere. Electric field distortion, if not corrected, impairs the gas multiplication effect and decreases collection of ionizing events occurring at the ends of the anode (Museum of Radiation and Radioactivity, 2022).

Unfortunately, the helix is susceptible to vibration which can result in microphonic noise (i.e., spurious counts) when moved during measurements. Neutrons interact with the A-150 tissue-equivalent wall of the TEPC producing recoil protons that ionize the tissue-equivalent (TE) gas to produce delta rays. Secondary electrons further ionize the TE gas resulting in a Townsend Avalanche producing an energy-dependent output pulse. The neutron recoil protons produced within the TEPC deposit energy based on two physical properties within the detector: the stopping power (directly proportional to the incident energy of the proton) and the distance traveled through the detector sphere (chord length). Photon and neutron interactions with the TE medium produce recoil protons and secondary electrons that contribute to the pulse height spectrum. The TEPC is designed and used to measure the frequency-averaged lineal energy ($\bar{y}_F$) and the dose-averaged lineal energy ($\bar{y}_D$) from the radiation energy deposited within the detector. Both lineal energy values are useful as the frequency-averaged lineal energy can be used for dose estimates and dose average lineal energy can be used to estimate the LET. The LET is an important quantity. Average LET corresponds to the value assigned to quality factors used in ICRP 60 to determine the dose equivalent in human tissue (ICRP, 1990). The radiation weighting factor from ICRP 103 was also used to describe the absorbed dose equivalent quantities to human tissue from the average neutron energy exposure from each neutron source sampled. Measuring energy deposited by neutrons in a TEPC will provide a better understanding of the biological impact that galactic cosmic radiation particles have on humans, especially those courageous enough to venture off into deep space.

BACKGROUND

Space Radiation

In the vacuum of space, astronauts are exposed to space radiation that is different from the radiation experienced on Earth. Space radiation consists of various atoms that travel near the speed of light, stripped of their electrons, with only the nucleus present. There are three main forms of space radiation that astronauts will be exposed to: solar wind particles trapped within planetary magnetic fields (e.g., Earth's Van Allen belts); solar particle events where stars (e.g., our sun) releases high-energy particles; and galactic cosmic radiation (GCR) from far away supernova explosions that release high energy protons and heavy ions of various elements (NASA, 2019). Missions beyond low Earth's orbit require upwards of 20 cm (or g cm^{-3}) water equivalent shielding to minimize the effects from these GCR and solar particle events.

Outside the Earth's magnetic field, astronauts traveling inside a spacecraft are exposed to a radiation environment consisting of GCR and solar radiation. GCR and solar radiation can deposit energy and ionize atoms as they pass through materials or tissue. The most likely exposures result from secondary charged or uncharged particles produced from inelastic interactions with spacecraft materials (NCRP 153, 2006). The combination of different radiation interactions results in an energy deposition in tissue and subcellular targets in human cells. The biological consequences of diverse energy deposition events remain a complex problem when defining exposure limits. Current exposure limitations for astronauts are in place to minimize harmful radiological effects from space exploration. The current dose limitations are based on keeping the mean risk of cancer mortality from exceeding a 3% increase in mean risk of cancer above the non-exposed population mean (NASA, 2022). According to NASA (2022), an

individual (accounting all ages and sexes) astronaut's total career effective radiation dose is limited to 600 mSv. Dose limits for one year and career non-cancer effects for human organs are outlined in Table 1.1.

Table 1.1 Astronaut Dose Limits (NASA, 2022)

Organ	1 Year Limit (Gy)	Career Limit (Gy)
Lens of Eye	2	4
Skin	3	6
Circulatory System	0.5	1
Central Nervous System	1	1.5

Human Tissue

Radiation induces damage in human cellular organelles, protein structures, RNA strands, and DNA in two methods, from direct energy absorption or reactive oxygen species produced during radiolysis of water inside the cell. The scope of biological damage resulting from radiation exposure depends on the radiation type and energy deposited in the target. Tissue target volumes where energy is deposited range a few microns to hundreds of microns. Different types of radiation deposit varying amounts of energy to the target material as they pass through. This process is defined by LET. Humans are normally exposed to low LET radiation such as photons and beta particles on Earth. Low LET radiation refers to types of radiation that deposit relatively less energy per unit length in a medium. Low LET radiation includes x-rays, gamma rays, and most types of beta particles. Low LET radiation has a longer range than high LET radiation and causes fewer ionizations per unit path length. Instead, low LET radiation primarily produces indirect effects through the generation of free radicals and reactive oxygen species via

interactions with water molecules in cells. Free radicals can cause damage to biological molecules.

High LET radiation in space is commonly in the form of HZE ions. HZE ions include alpha particles, heavy ions (e.g., iron ions), and neutrons. High LET radiation has a short range and causes numerous densely packed ionizations and excitations along its path. The HZE dense ionization pattern leads to a higher probability of direct damage to biological molecules, including DNA, and can result in more severe biological effects than low LET radiation. Lower doses from high LET exposures induce more harmful effects compared to similar dose low LET radiation. High LET radiation passing through DNA can induce genomic lesions or clustered DNA damage that involve single or double strand breaks, base substitutions, and cross linkage (Meerman, 2021). If DNA alterations are not promptly repaired by the cell, the lesions may result in sustained mutations, carcinogenesis, random chromosomic recombination, or death.

According to ICRP 133 (2016), neutrons interact with human tissue through four main processes: neutron capture, elastic scattering, inelastic scattering, and nuclear reactions. Neutron capture is the dominant interaction at lower energies. The emission of 2.2-MeV photons resulting from the capture of thermalized neutrons with hydrogen atoms from $^{1}H(n, \gamma)^{2}H$ reactions contribute to significant energy deposition in the body. The $^{14}N(n, p)^{14}C$ reaction, producing ~600 keV protons, also contributes to absorbed dose. Above 1 keV, recoil protons from elastic scattering with hydrogen atoms deposit substantial energy. Inelastic scattering involves reactions with energy thresholds where neutrons lose energy, exciting nuclei to emit photons without charged particle emission. Inelastic scattering only accounts for a small percentage of the total absorbed dose in body tissue. At energies above a few MeV, the production of charged particles through nuclear reactions becomes increasingly significant in energy deposition.

The human body is capable of withstanding significant radiation exposures before incurring adverse long term effects or deterministic effects. Untoward effects of radiation are strongly associated with high dose, short term exposures, and in space, severe acute exposures from GCR or solar events may result in harmful effects to an astronaut. Cardiovascular tissue is sensitive to radiation effects and is the reason why astronauts have lower dose limitations for the circulatory system (Table 1.1). Exposure to various types of space radiation such as GCR and solar particles can lead to radiation-induced cardiovascular disease, resulting in the development of cardiovascular disease or the aggravation of existing disease. Radiation-induced cardiovascular disease such as acute pericarditis can develop from a short-term exposure or develop into chronic radiation-induced cardiovascular disease over a longer period of time. Chronic radiation-induced cardiovascular disease is progressive and includes multiple disorders of the cardiovascular system, such as accelerated development of atherosclerosis, myocardial remodeling and fibrosis, valve abnormalities, cardiomyopathies, arrhythmias, and other related disorders (Meerman, 2021). Because high LET space radiation is a common exposure in deep space, studying the effects of radiation on cardiovascular cells and tissue will help determine the overall harmful effects to humans traveling in space. With the purpose of exploring potential dosimetric disparities between mixed LET environments generated by photons and neutrons, the main study seeks to measure and compare TEPC dose-equivalent rates in microdosimetric volumes. The findings from this experiment revealed that when both photons and neutrons interacted with the TEPC, the mixed LET environments displayed lower LET values in comparison to neutron-only exposures. Moreover, these mixed environments yielded varying dose equivalent rates that relied on the characteristics of the radiation source.

METHODS AND MATERIALS

Detector Information

Neutrons were measured using a LET-½" spherical TEPC (Serial No. 1217 and 1373) (Far West Technology, Inc., Goleta, CA). The detector is suitable for measuring neutron spectra lineal energy, y (keV μm^{-1}). Pulse height distribution from neutron interactions within the TEPC were used to estimate the equivalent dose rate to human tissue utilizing quality factors based on the measured dose-average LET. The detector housing is a thin aluminum shell (0.0178 cm thick) which serves as a vacuum-tight housing and provides electrostatic shielding. The active volume of the detector is 1.27 cm in diameter and has a 0.127 cm thick wall of TE plastic. The detector stem has a connector block at one end carrying the high voltage, signal connectors, and a vacuum fitting. The TEPC is designed to be evacuated and filled with TE proportional counting gas at low pressure, typically 25 to 400 torr. The low-pressure tissue equivalent gas enables the TE gas volume to simulate small tissue volumes from less than 1 to more than 8 microns in diameter. However, exceeding 3 microns simulated volumes results in quenching from the fill gas (propane) used within the detector. Figures 2.1 and 2.2 showcase the TEPC and its internal design. Table 2.1 provides technical specifications of the detector, calibration source and the propane gas composition used.

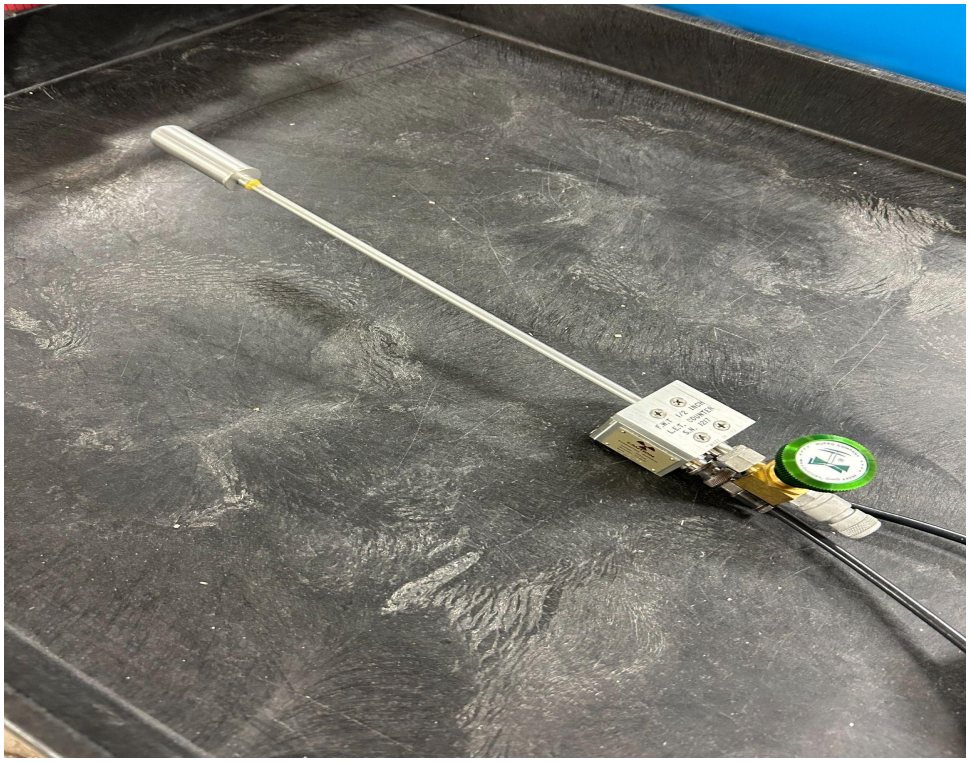

Figure 2.1 ½" TEPC Detector

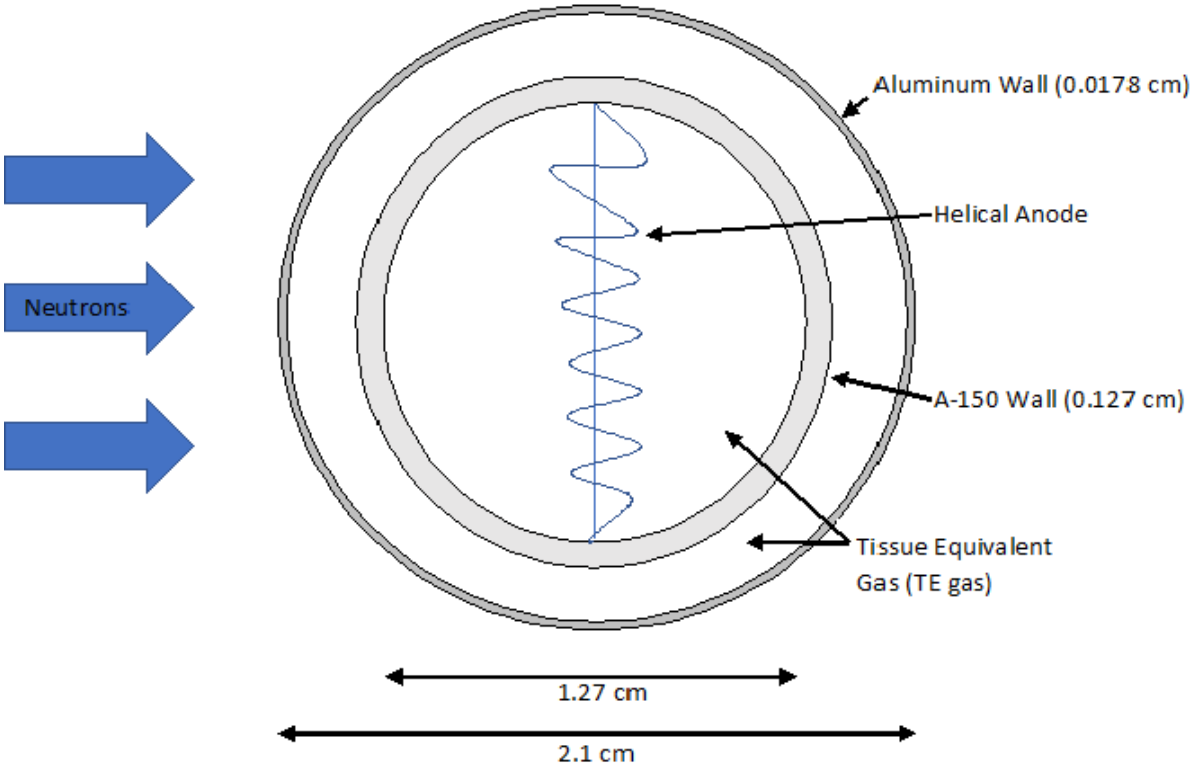

Figure 2.2 ½" TEPC Internal Diagram

Table 2.1 Technical Specifications for LET-½" TEPC

½" LET TEPC Specifications	
TE Diameter	1.27 cm
Shonka Type A-150 Plastic Density	1.12 g cm^{-3}
TE Wall Thickness	0.127 cm
Detector Diameter (Max)	2.1 cm
Al Detector Wall Thickness	0.0178 cm
^{244}Cm Calibration Source	5.8 MeV Alpha Particle, <0.3 μCi (11.1 kBq)
TE Gas Composition	C_3H_8:CO_2:N_2 (55.004:39:5.996)
TE Gas Molecular Weight	43.1 g mol^{-1}

Tissue Equivalent Simulation

The TEPC is pressurized to an internal pressure that will ensure the same number of tissue molecules are present in a less dense medium as is present in a typical human cell to simulate a microdosimetric volume of tissue. For this experiment, a very low-pressure propane gas mixture was pumped into the detector to simulate volumes of tissue from 1 to 2 μm. The internal pressure inside the detector will correlate to the simulated diameter being sampled. The tissue equivalent gas pressure density needed is determined using Equation 2.1:

$$\rho_t \cdot d_t = \rho_{gas} \cdot d_{gas} \qquad \textbf{Equation 2.1}$$

Where: ρ_t = density of tissue (g cm^{-3})

d_t = diameter of simulated tissue volume (μm)

ρ_{gas} = density of TE gas (g cm^{-3})

d_{gas} = diameter of TE gas volume (μm)

The relationship in Equation 2.1 can be applied to the Ideal Gas Law when determining the TEPC's internal gas pressure, P_{gas}, and is shown in Equation 2.2.

$$P_{gas} = \frac{\rho_{gas}}{MW} \cdot R \cdot T \quad \text{[torr]} \qquad \textbf{Equation 2.2}$$

Where: P_{gas} = gas pressure (torr)

$R = 62,364$ (cm^3 torr mol^{-1} K^{-1})

T = temperature (Kelvin)

MW = molecular weight of fill gas (g mol^{-1})

The LET-½" TEPC detector was filled with 34.7 torr and 69.4 torr of propane gas mix to simulate 1 μm and 2 μm of tissue, respectively. The molecular weight of the propane gas mix was 43.1 g mol^{-1}, at a room temperature of 293 K. Figure 2.3 shows the pump station used to produce the vacuum and pressurize the TEPC with the propane-mixed gas. The detector was initially depressurized using an IDP3 vacuum pump (Agilent Technologies, Santa Clara, CA) to remove residual air. The vacuum connection was closed off upon depressurization and propane gas mix was introduced to the detector. Next, the vacuum connection was reopened to reduce internal gas pressure to the desired value. The vacuum and re-pressurization step to replenish the gas used within the detector is important to repeat to ensure the purity of the gas in the TEPC. A small digital DCP 3,000 vacuum gauge (Vacuubrand, Essex, CT) was used to measure the system's internal pressure in torr.

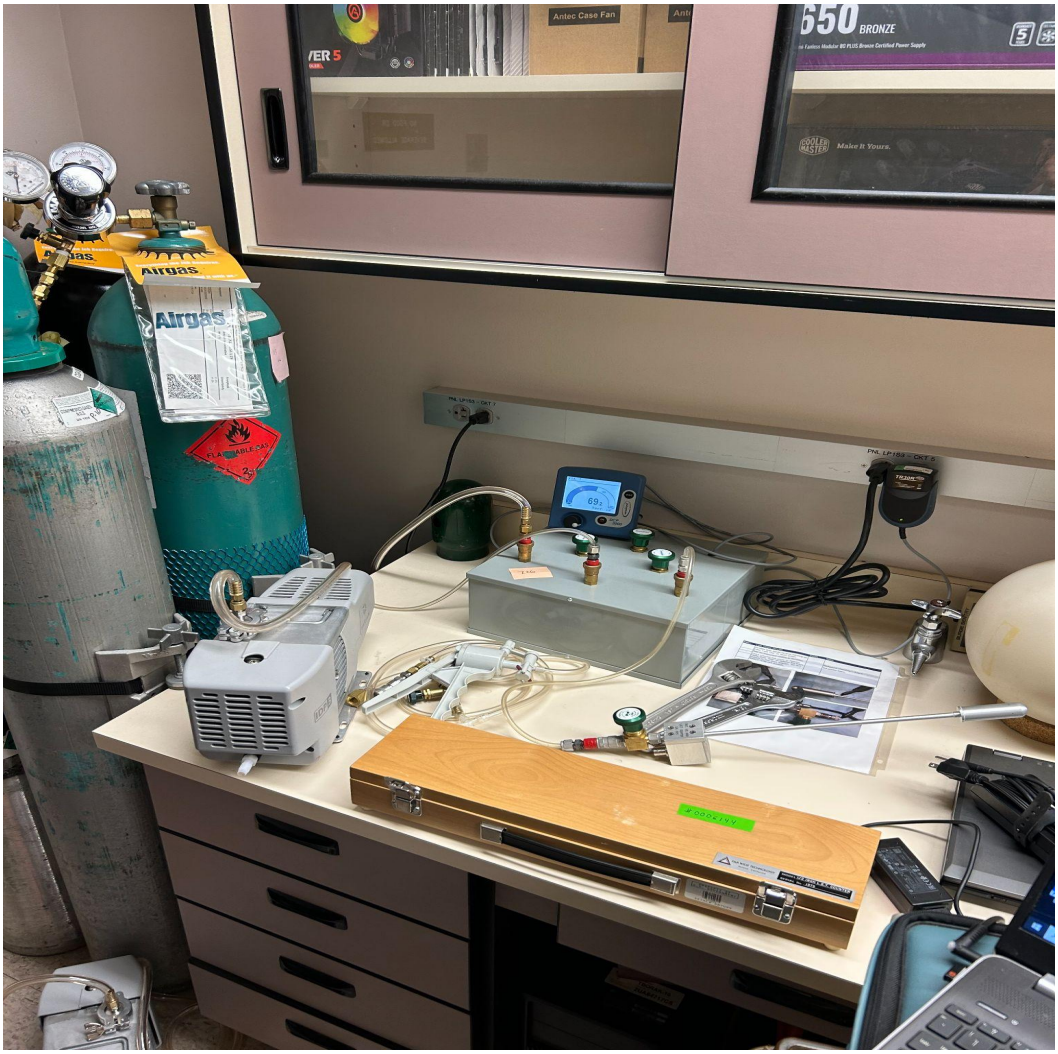

Figure 2.3 Pump Station

Electronic Setup

The LET-½" TEPC was used to conduct spectral measurements of neutrons. The TEPC was filled to the pressures 34.7 torr and 69.5 torr of propane gas mix to simulate 1 µm and 2 µm of tissue, respectively. The TEPC was connected to an ORTEC 142AH preamplifier (ORTEC/AMETEK, Oak Ridge, TN) and Tennelec TC 954A high voltage power supply (Tennelec, Oak Ridge, TN) at 580 V for 1 µm or 600 V for 2 µm simulated diameter. The voltage supply was set to the recommended settings based on the manufacturer's guidance. The signal from the preamplifier was transmitted to an ORTEC 572A shaping amplifier

(ORTEC/AMETEK, Oak Ridge, TN) with a 3 µs shaping time, x1 fine gain, and x20 course gain. The input signal was set to receive positive pulse polarity only. A Tektronix TDS 3012 oscilloscope (Danaher Corporation, Washington, DC) was used to monitor the waveform of electronic signals being received from the detector and amplifiers and ensure positive pulse polarity. TEPC signals from the amplifier were then processed with a SPECTECH UCS 30 multichannel analyzer (MCA) (Spectrum Techniques, Oak Ridge, TN) where the output signals were subject to pulse height analysis on USX V1.2 software (Spectrum Techniques, Oak Ridge, TN). The settings on the UCS 30 MCA were 1,049 channel display, x2.49 fine gain, and x2 course gain to plot the data evenly on the spectrum. Figure 2.4 outlines the electronic setup of the detector and equipment used to take the spectral measurements in this experiment. Data was collected, energy calibrated, and analyzed before importing them into an Excel spreadsheet (Microsoft, Redmond, WA). Some samples required 18 to 23 hours to accumulate sufficient data for spectral analysis depending on neutron fluence of the source. Lastly, the detector was placed in a perpendicular orientation to the source.

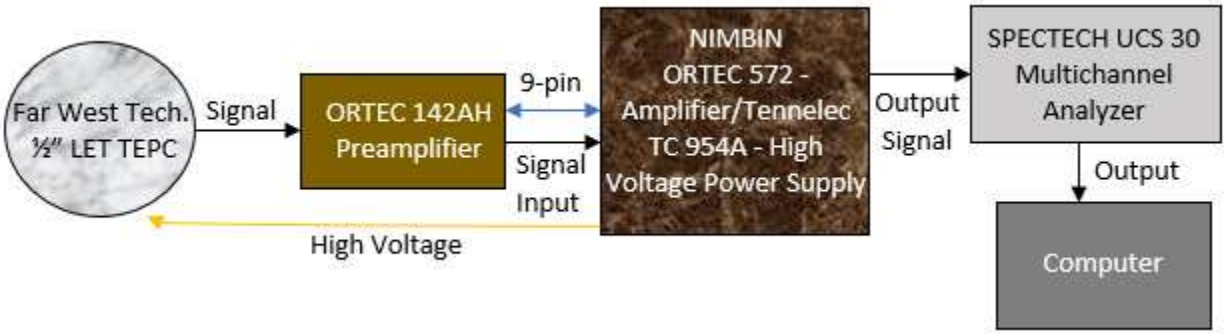

Figure 2.4 Electronic Setup

Energy Calibration

An energy calibration was performed before each sampling event to ensure the data set measurement comparability. Energy calibration assigns a known energy to a channel number

from the pulse height distribution. The TEPC contains a gravity-activated source of ^{244}Cm (<0.3 μCi or 11.1 kBq on May 1995) that emits alpha particles at 5.8 MeV (Borak, 2019/NNDC, n.d.). Alpha particles are collimated along a trajectory through the center of the gas cavity from the ^{244}Cm source when exposed. The fixed stopping power of the alpha particle traveling the cavity provides a clear calibration for the gain of the proportional counter. The main peak generated represents the signal from the alpha particles traversing a length corresponding to the diameter of the detector. The associated channel number is then assigned an energy deposition corresponding to LET_{α} = 81.72 keV μm^{-1} over a range of 1 μm in tissue (Far West Technology, n.d.). Depending on the simulated diameter being tested, the LET_{α} multiplied by the simulated diameter becomes energy deposited (keV). The energy calibration process is used to calculate the deposited energy (ε) per channel as follows:

$$\varepsilon_i = \frac{81.72 \cdot Y}{X} \quad [\text{keV ch}^{-1}] \qquad \textbf{Equation 2.3}$$

Where: X = the channel number of the alpha peak

Y = the simulated diameter (μm)

Figure 2.5 shows an energy calibration peak from the ^{244}Cm source after 2 minutes exposure. An energy calibration is performed before starting a new sample event or after re-pressurizing the detector. Recalibrating the detector every 8 hours is important due to channel shift from pressure changes within the detector.

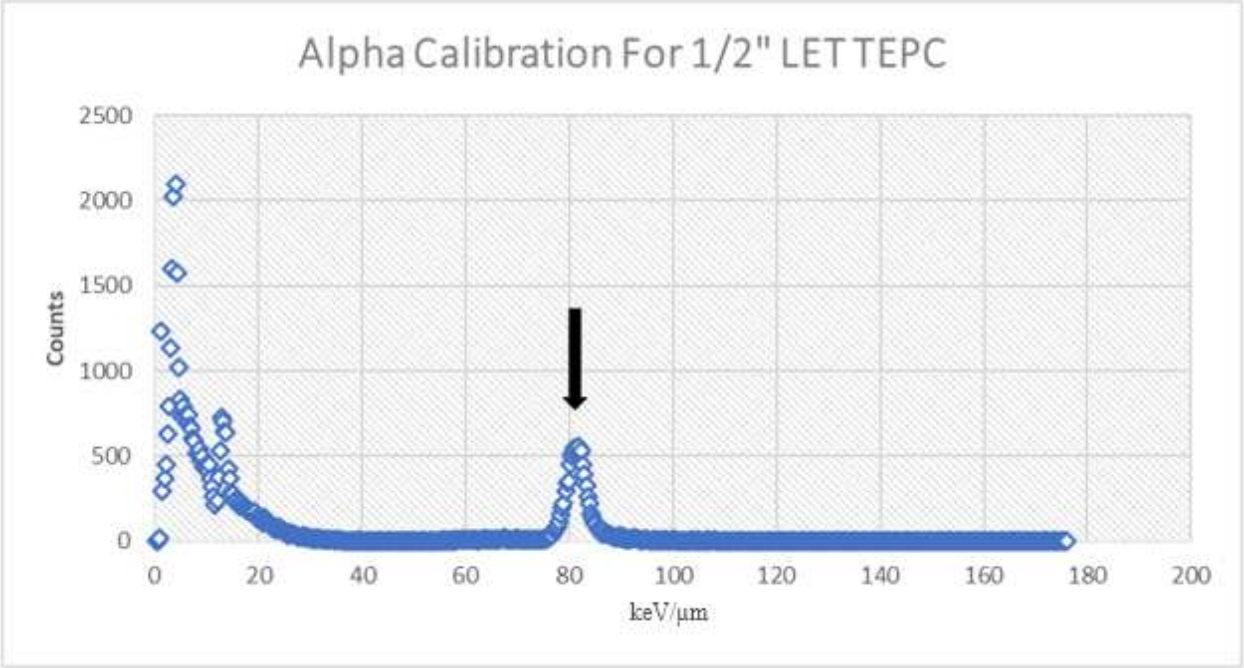

Figure 2.5 Alpha Calibration for ½" LET TEPC

Plutonium Beryllium (^{239}PuBe) Neutron Source

The PuBe neutron source is secured inside a Model NH-3 Neutron Howitzer (Serial # 43) (Nuclear Chicago Corporation, Wheaton, IL) shown in Figure 2.6. The PuBe source specifications are listed in Table 2.2. The plutonium-239 within the PuBe mixed source has a half-life of 24,110 years and was manufactured in 1967. The 5 curie (185 GBq) PuBe source emits isotropic neutrons at an average energy of 4.6 MeV with a maximum emission rate of 6.5 × 10^6 neutrons per second. The PuBe source is 18.4 cm long with a diameter of 2.86 cm and is attached to a lucite rod, 49.2 cm long (Corporation, 1963). Neutron production in the plutonium and beryllium source is according to these interactions:

$$^{239}_{94}Pu \rightarrow \ ^{235}_{92}U + \ ^{4}_{2}He$$

$$^{9}_{4}Be + \ ^{4}_{2}He \rightarrow \ ^{13}_{6}C^{*}$$

$$^{13}_{6}C^{*} \rightarrow \ ^{12}_{6}C + \ ^{1}_{0}n \text{ (Branching Ratio = 40\%)}$$

$$^{13}_{6}C^{*} \rightarrow \ ^{12}_{6}C + \ ^{1}_{0}n + \gamma\,(4.4\,MeV)$$ (Branching Ratio = 60%)

Table 2.2 PuBe Source Specifications

Initial Source Activity	5 Ci (185 GBq) on 1967
Half life	24,110 years
Average Neutron Energy	4.6 MeV
Max Neutron Yield	6.5×10^{6} n sec^{-1}
Neutron Fluence at 15 cm	2.3×10^{3} n cm^{-2} sec^{-1}

Figure 2.6 Neutron Howitzer - PuBe Housing

Deuterium-Tritium (DT) Neutron Source

The DT110-14 MeV Neutron Generator (Adelphi Technology, Inc., Redwood City, CA) is a sealed, high-output neutron generator utilizing a DT reaction to produce 14.1 MeV neutrons

(Adelphi Technology, n.d.). Figures 2.7 and 2.8 depict the neutron generator and its setup. The DT neutron generator is based on a nuclear reaction between two hydrogen isotopes, deuterium, and tritium. Tritium is a radioactive gas, so the DT generator is sealed to contain the gas. The DT interaction and the production of neutrons occur according to this interaction:

$$ {}_{1}^{2}H + {}_{1}^{3}H \rightarrow {}_{2}^{4}He + {}_{0}^{1}n $$

The neutron generator requires 500 W to operate and single phase 110 V with a 20 A electricity supply. The generator is computer controlled via a graphical user interface and has a series of hardware safety interlocks for the protection of personnel and the generator itself. The neutrons generated are dependent on the amount of tritium available, therefore, the performance degrades after several thousand hours of operation. The generator can be pulsed or in continuous operation producing a maximum output of 10^{10} neutrons per second when operated at 60 kV and 1.6 mA (Adelphi Technology, n.d.). Since DT neutrons have an energy of 14.1 MeV, the neutrons penetrate objects which is an important consideration in shielding. DT-produced neutrons are significantly more energetic and require more material to moderate and absorb compared to PuBe or ^{252}Cf neutrons. Table 2.3 identifies the specific parameters of the operation and activity of the DT neutron generator.

Table 2.3 DT 110 Specifications

Neutron Energy	14.1 MeV
DT Neutron Yield	1×10^{10} n sec^{-1}
Neutron Fluence at 214 cm	1.7×10^{4} n cm^{-2} sec^{-1}
Operating Voltage	~60 kV
Operating Current	~1.60 mA
Operating Mode	Continuous

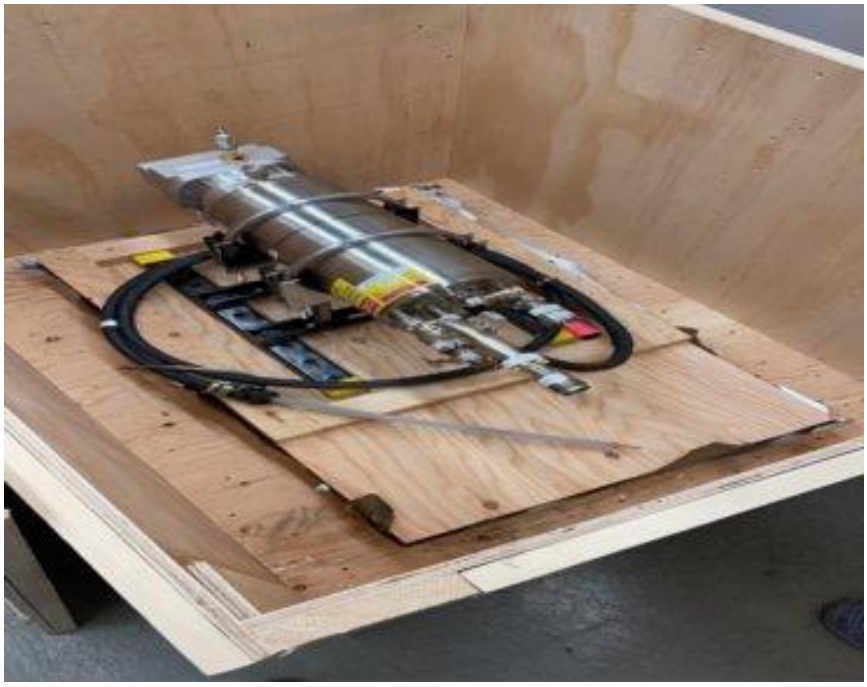

Figure 2.7 DT 110-14 MeV Neutron Generator

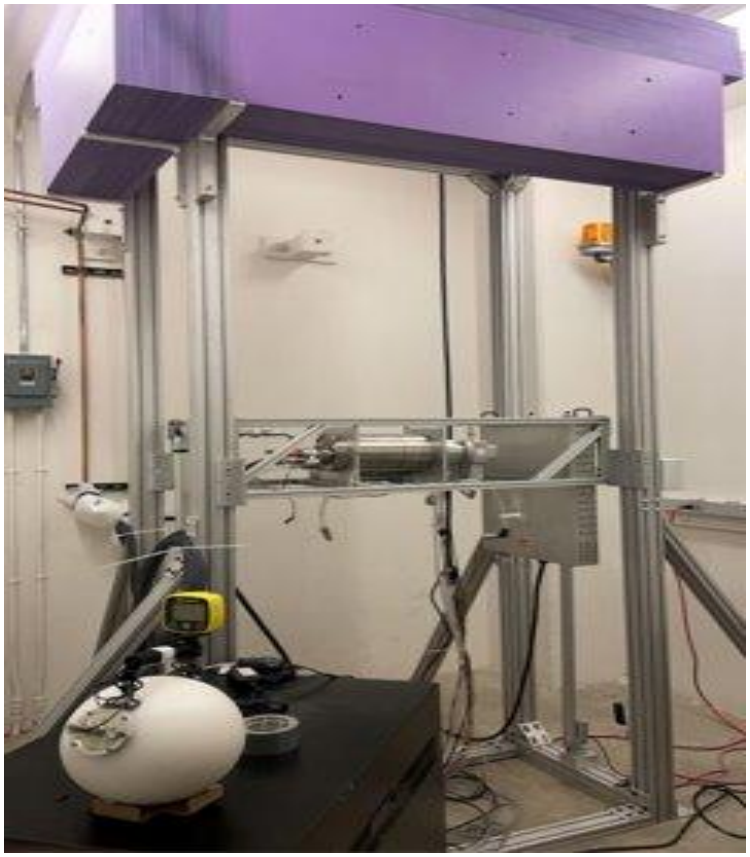

Figure 2.8 Neutron Generator Configuration

Facility Design

The neutron generator and PuBe source are stored and operated in the basement of the Molecular and Radiological Biosciences building at Colorado State University. The facility is built with 6" concrete walls (15.24 cm) and is designed to house radioactive sources. Figure 2.9 illustrates the facility layout and placement of the sources and equipment within the room.

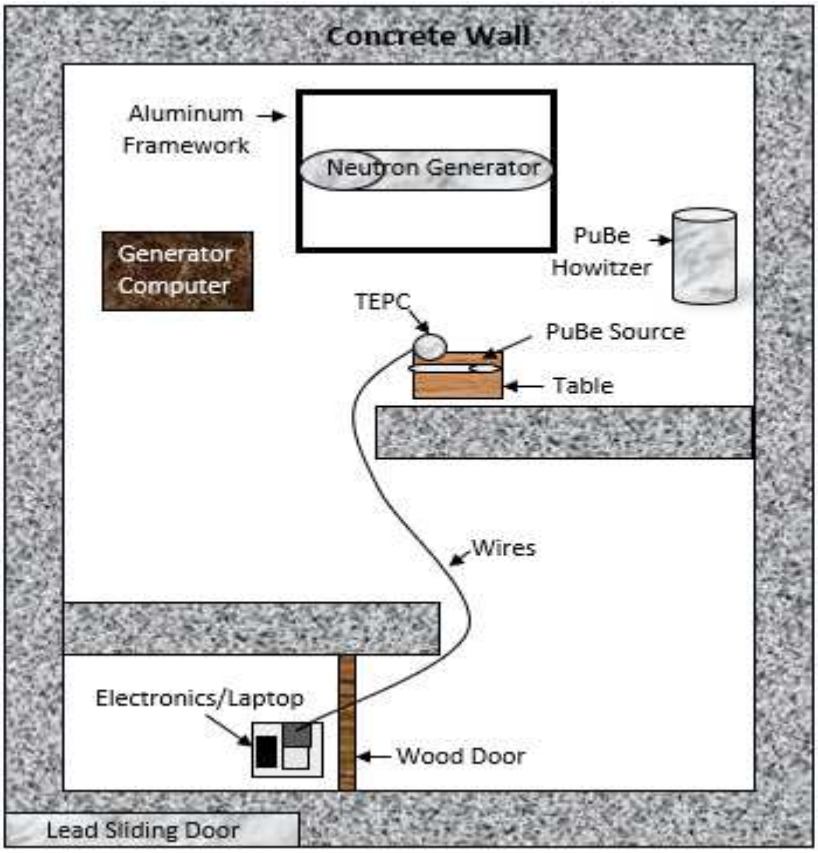

Figure 2.9 Facility Layout

Californium-252 (^{252}Cf) Neutron Source

The neutron irradiator (Model 149, SN: 12036) (J.L. Sheppard & Associates , San Fernando, CA), located at Colorado State University's Foothills campus, contains a sealed source of ^{252}Cf (9.44 mCi between 3-6 Jan 23) housed in a panoramic irradiator capable of long periods of operation. The neutron irradiator is housed inside a shielded chamber as shown in Figure 2.10.

The foothills facility was built to conduct low-dose rate, mixed LET field radiation exposure studies on rodents using dose rates and total doses relevant for extended manned missions in space (Borak, 2019). Studies have shown that exposure to fission spectrum neutrons results in quantitative and qualitative carcinogenic effects similar to HZE observed in space. The panoramic irradiator utilizes a 1-inch lead shield to minimize gammas from interfering with neutron exposure studies. Californium-252 alpha decays into ^{248}Cm 97% of the time, however, 3% of the decays will spontaneously fission releasing low to high-energy neutrons ranging from 0.5 to 13 MeV. The neutron yield for ^{252}Cf is 2.314×10^6 n μg^{-1} sec^{-1} with an average neutron energy of 2.1 MeV (Borak, 2019). Table 2.4 outlines the source specifications of the neutron irradiator and includes the neutron fluence at 1 meter.

Table 2.4 Neutron Irradiator (^{252}Cf Source) Specifications

Initial ^{252}Cf Source Activity	81.8 µg (43.82 mCi) on 28 Feb 2017
Decay Corrected Activity	17.6 µg (9.44 mCi) between 3-6 Jan 2023
Half life	2.645 years
Specific Activity	536 µCi μg^{-1}
Average Neutron Energy	2.1 MeV
Most Probable Neutron Energy	0.7 MeV
Neutron Yield	2.314×10^6 n μg^{-1} sec^{-1}
Neutron Fluence at 100 cm	3.2×10^2 n cm^{-2} sec^{-1}

Figure 2.10 Neutron Irradiator

Lineal Energy Measurements

Lineal energy derived calculations for frequency-mean lineal energy, dose-mean lineal energy, and LET are based on ICRU 36 (1983). Lineal energy (y) is defined as the quotient of the energy imparted (ε) to the matter in a volume from a single energy deposition event by a mean chord length (l) in that volume, as shown below:

$$y = \frac{\varepsilon}{\bar{l}} \quad [\text{keV } \mu\text{m}^{-1}] \qquad \textbf{Equation 2.4}$$

The lineal energy is a microscopic analog of the LET. The mean chord length within the spherical cavity from the simulated diameter (Y) is derived as $\frac{2}{3}Y$. The lineal energy is determined from the imparted energy per channel (ε) by the mean chord length based on the simulated diameter. Therefore, the lineal energy per channel is:

$$y_i = \frac{\varepsilon_i}{\frac{2}{3} \cdot Y} \quad [\text{keV } \mu\text{m}^{-1}\text{ ch}^{-1}] \qquad \textbf{Equation 2.5}$$

The expectation value of the lineal energy distribution (Equation 2.6) is called frequency-mean lineal energy ($\bar{y}_F$) and is represented by:

$$\bar{y}_F = \int_0^\infty y_i \cdot f(y)dy \quad [\text{keV } \mu\text{m}^{-1}] \qquad \textbf{Equation 2.6}$$

The absorbed dose distribution d(y) with respect to a lineal energy distribution can also be considered. The expectation value of the absorbed dose distribution with a lineal energy described as follows is called dose-mean lineal energy ($\bar{y}_D$), as provided below:

$$\bar{y}_D = \int_0^\infty y \cdot d(y)dy = \frac{1}{\bar{y}_F}\int_0^\infty y^2 \cdot f(y)dy \quad [\text{keV } \mu\text{m}^{-1}] \qquad \textbf{Equation 2.7}$$

The frequency-mean lineal energy, $\bar{y}_F$ by considering a single-energy deposition event distribution from the multichannel analyzer counts per channel can be rewritten as follows:

$$\bar{y}_F = \int_0^\infty y_i \cdot f(y)dy \equiv \frac{1}{n}\sum_i n_i \cdot y_i \qquad \textbf{Equation 2.8}$$

$$f(y) = \frac{n_i}{\Sigma n_i} \quad [\text{keV } \mu\text{m}^{-1}]$$

Where, n_i is the number of counts of a single-energy deposition event per channel, (y_i) is the lineal energy per channel. Likewise, the dose-mean lineal energy $\bar{y}_D$ can also be obtained from the lineal energy distribution data using Equation 2.9:

$$\bar{y}_D = \frac{1}{\bar{y}_F}\int_0^\infty y^2 \cdot f(y)dy \equiv \frac{\Sigma n_i \cdot y_i^2}{\Sigma n_i \cdot y_i} \quad [\text{keV } \mu\text{m}^{-1}] \qquad \textbf{Equation 2.9}$$

According to Kellerer (1972), the dose-average LET and the dose average lineal energy, $\bar{y}_D$, are important quantities for practical applications when considering the radiations's contribution to the local dose. The dose-average LET is roughly 8/9ths of the lineal energy

distribution in spherical detectors. Therefore, the dose-mean lineal energy ($\bar{y}_D$) is used to calculate the dose-average LET and is represented by Equation 2.10:

$$LET = \frac{8}{9} \cdot \bar{y}_D \quad [\text{keV } \mu\text{m}^{-1}] \qquad \textbf{Equation 2.10}$$

The quality factor (Q) can be calculated utilizing the dose-average LET. The quality factor characterizes the biological effectiveness of a radiation type and is based on the ionization density along the tracks of charged particles in tissue (ICRP, 1990). The quality factor is a dimensionless modifier and is defined as a continuous function of the LET, detailed in Table 2.5. The quality factor has been superseded by the radiation weighting factor in the definition of equivalent dose, but is still used in calculating the operational dose equivalent quantities used in monitoring (ICRP, 2007). The neutron radiation weighting factors (w_R) for dose-equivalent calculations are shown in Table 2.6, which focuses on the neutron energy (E_n) rather than the LET.

Table 2.5 ICRP 60 Quality Factor (Q) vs. LET (L) Relationship

LET (L)	Quality Factor (Q)
$L < 10$ keV μm^{-1}	1
$10 \leq L \leq 100$ keV μm^{-1}	$0.32 \cdot L - 2.2$
$L > 100$ keV μm^{-1}	$300 \cdot L^{-1/2}$

Table 2.6 ICRP 103 Neutron Radiation Weighting Factor (w_R)

E_n	w_R
$E_n < 1$ MeV	$2.5 + 18.2\, e^{-\frac{[ln(En)]^2}{6}}$
1 MeV $\leq E_n \leq$ 50 MeV	$5.0 + 17.0\, e^{-\frac{[ln(2 \cdot En)]^2}{6}}$
$E_n > 50$ MeV	$2.5 + 3.25\, e^{-\frac{[ln(0.04 \cdot En)]^2}{6}}$

Calculating Absorbed Dose, Fluence, and Dose Equivalent

If the TEPC is in charged particle equilibrium when irradiated by fast neutrons, the absorbed dose measured by the TEPC can be calculated using Equation 2.11:

$$\text{Absorbed Dose} = \frac{d\varepsilon}{dm} = \frac{1.602\times10^{-13}}{\rho_{gas}\cdot V_{gas}}\sum_i n_i \cdot \varepsilon_i = \frac{1.602\times10^{-13}}{m_{gas}} \cdot \frac{2Y}{3}\sum_i n_i \cdot y_i \quad \text{[Gy]} \qquad \textbf{Equation 2.11}$$

Where: ε = energy deposited in the TEPC (keV)

1.602×10^{-13} = conversion constant (Gy-g keV^{-1})

Y = simulated diameter (μm)

ρ_{gas} = density of TE gas (g cm^{-3})

V_{gas} = volume of TE cavity (cm^3)

m_{gas} = mass of TE gas (g)

The absorbed dose rate was calculated based on the dose measured from the detector divided by the live time (real-time - dead time) converted to hours. The absorbed dose from each neutron source varies based on distance from the source, exposure time, and shielding materials used. Distance from the source (x) will change the neutron fluence interacting with the TEPC. Equation 2.12 was used to calculate neutron fluence for each source:

$$\text{Neutron Fluence (n cm}^{-2}\text{ sec}^{-1}) = \frac{N}{4\cdot\pi\cdot x^2} \qquad \textbf{Equation 2.12}$$

Where: x = distance from the surface of the source to the detector (cm)

N = maximum neutron yield of the source (n sec^{-1})

The neutron fluence will influence the absorbed dose rate measured on the TEPC. A longer exposure time will increase the likelihood of capturing neutron interactions from higher energies. Shielding materials used reduce unwanted radiation such as gamma rays from ionizing the A-150 wall, but may also scatter neutrons in the process.

Using the absorbed dose (D) and the respective quality factor (Q), the dose equivalent (H) can be determined, using Equation 2.13:

$$H = D \cdot \mathrm{Q} \qquad [\mathrm{Sv}] \qquad \textbf{Equation 2.13}$$

The dose equivalent is a measurement of biological damage to living tissue as a result of radiation exposure. Short and long-term dose effects can be estimated based on the dose equivalent quantities.

RESULTS

PuBe Neutron Interactions

TEPC measurements for the PuBe neutron source resulted in diverse interactions due to the characteristics of the source. Figures 3.1 - 3.6 illustrate the PuBe neutron/gamma interactions and the lineal energy distribution for the neutron field produced. Measurements were taken with and without lead shielding to determine the influence of photons on the spectrum. Two inches of lead were used to shield the 4.4 MeV capture photons produced from the excited $^{13}C^{*}$ product from the ^{9}Be and ^{4}He reaction. Table 3.1 outlines the frequency-mean lineal energy ($\bar{y}_F$), dose-mean lineal energy ($\bar{y}_D$), dose-average LET, and absorbed dose rate calculated from the measurements obtained from sampling the PuBe source. Sources with and without shielding were sampled between 19 to 20 hours.

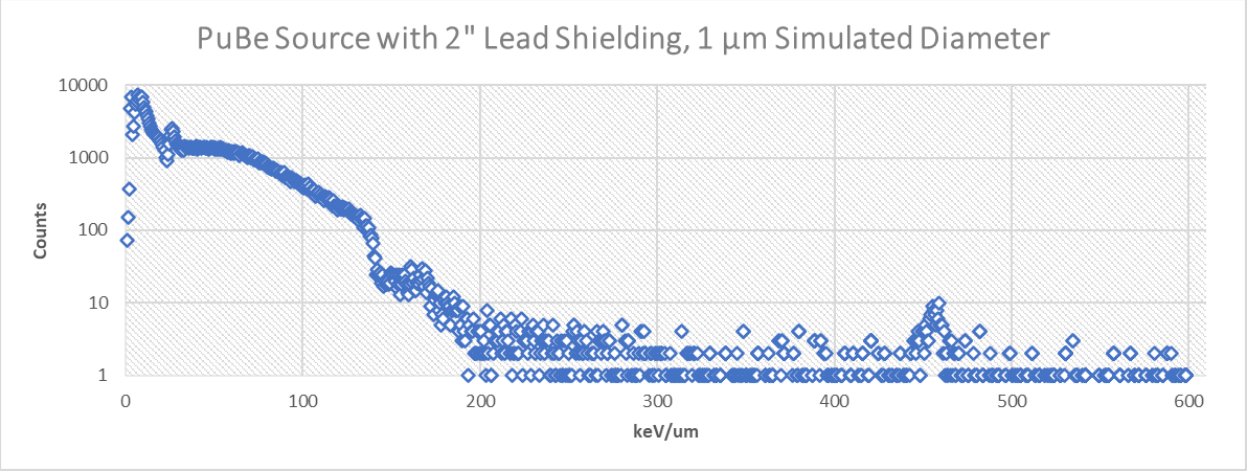

Figure 3.1 PuBe Source with 2" Lead Shield, 1 µm Simulated Diameter

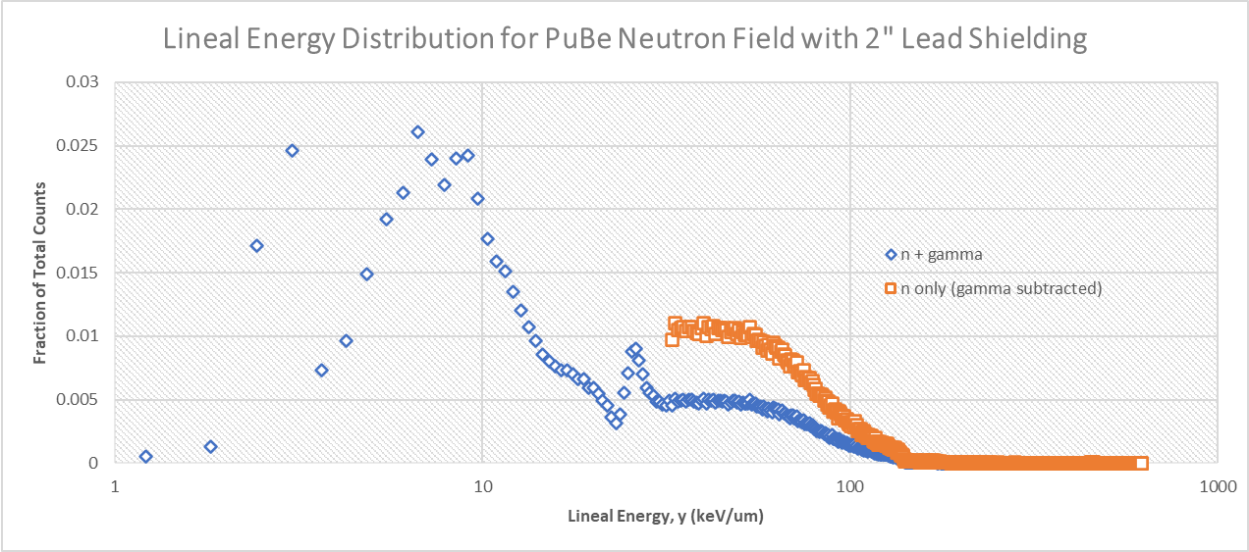

Figure 3.2 Lineal Energy Distribution for the PuBe Neutron Field with 2" Lead Shield, 1 µm Simulated Diameter

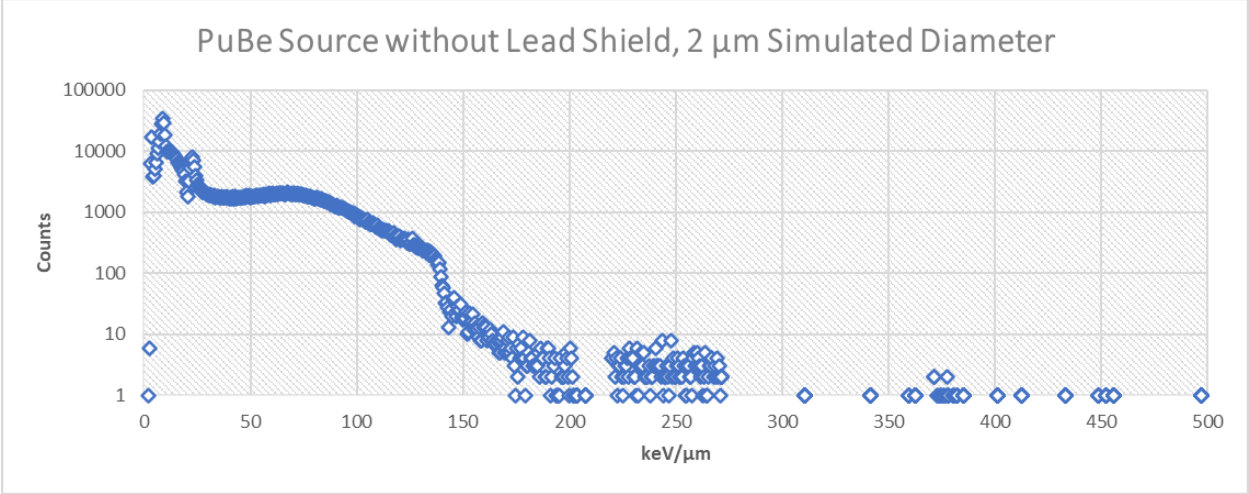

Figure 3.3 PuBe Source without Lead Shield, 2 µm Simulated Diameter

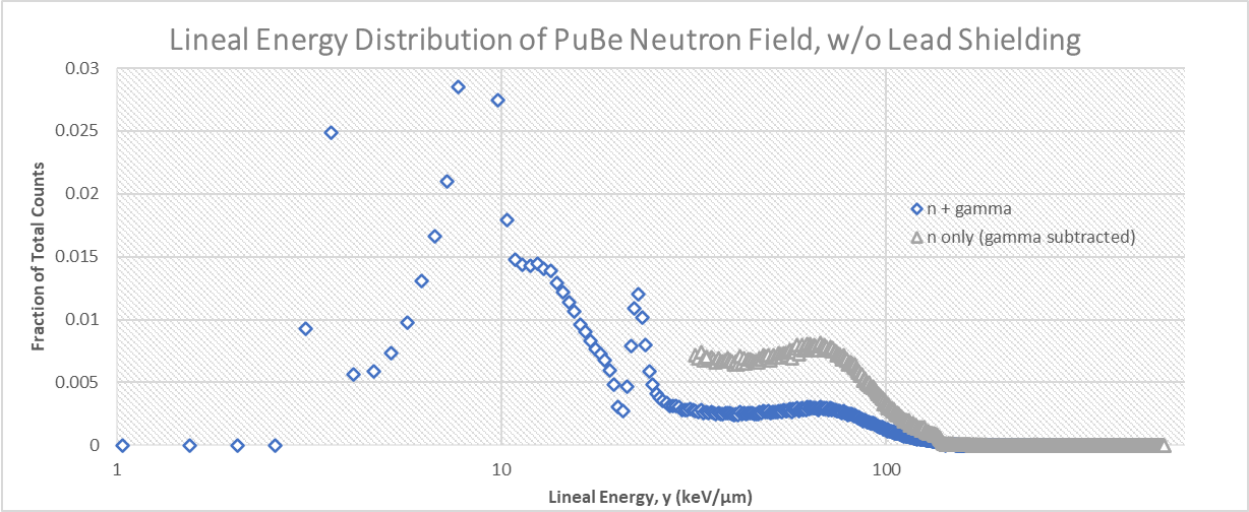

Figure 3.4 Lineal Energy Distribution for the PuBe Neutron Field without Lead Shielding, 2 µm Simulated Diameter

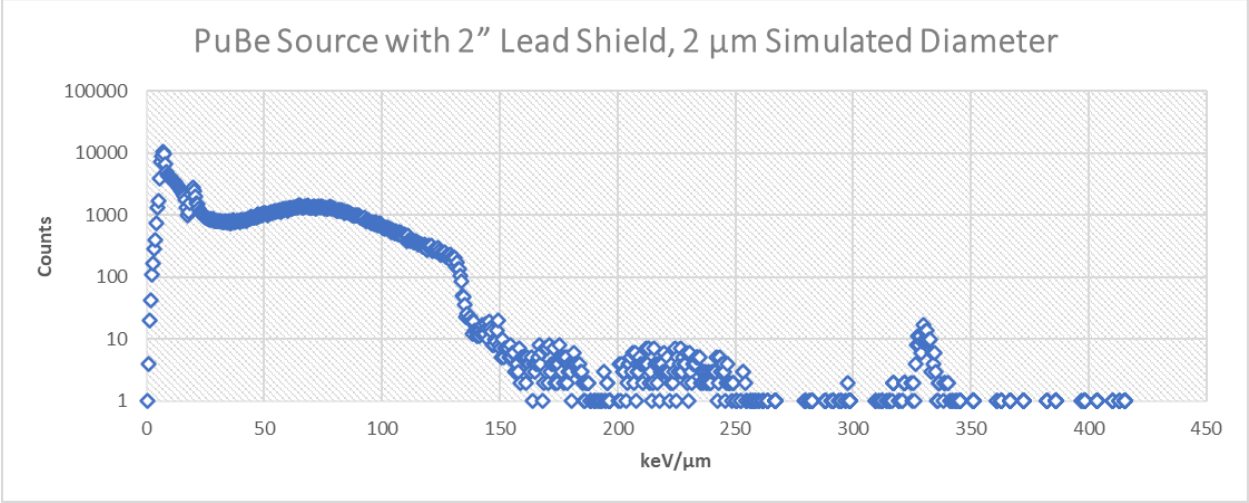

Figure 3.5 PuBe Source with 2" Lead Shield, 2 µm Simulated Diameter

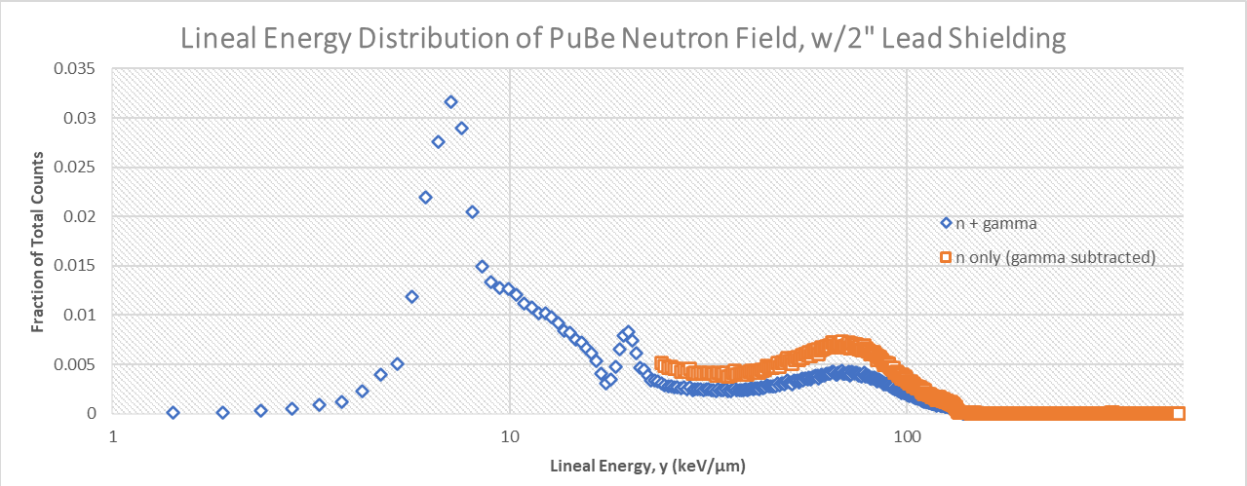

Figure 3.6 Lineal Energy Distribution for the PuBe Neutron Field with 2" Lead Shielding, 2 µm Simulated Diameter

Californium-252 Neutron Interactions

Californium-252 creates a mixed LET environment producing both neutrons and gamma radiation through spontaneous fission. Figures 3.7 - 3.12 illustrate the ^{252}Cf fission neutron/gamma interactions, and the lineal energy distribution for the neutron field produced. Measurements were taken with and without lead shielding to determine the influence of photons on the spectrum. One-inch lead shielding was fixed to the irradiator to shield the low-energy photons being produced by the ^{252}Cf source. To sample the low-energy photons, the detector was placed below the lead shielding. Additional tests were conducted to determine differences in TEPC interaction based on the simulated tissue diameter. Table 3.1 outlines the frequency-mean lineal energy ($\bar{y}_F$), dose-mean lineal energy ($\bar{y}_D$), dose-average LET, and absorbed dose rate calculated from the measurements obtained from sampling the ^{252}Cf source. Source sampling with and without shielding, at 2 µm simulated diameter, was conducted for 22.8 and 22.7 hours, respectively. The 1 µm simulated diameter sample exposed to the source, with shielding, was sampled for 22.6 hours.

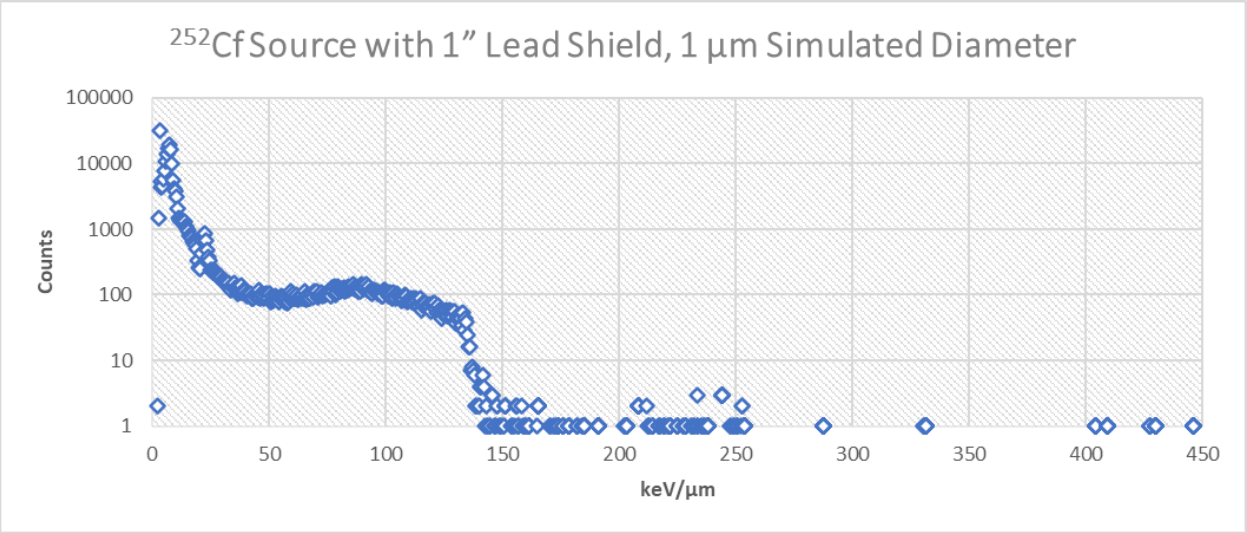

Figure 3.7 ^{252}Cf Source with 1” Lead Shield, 1 µm Simulated Diameter

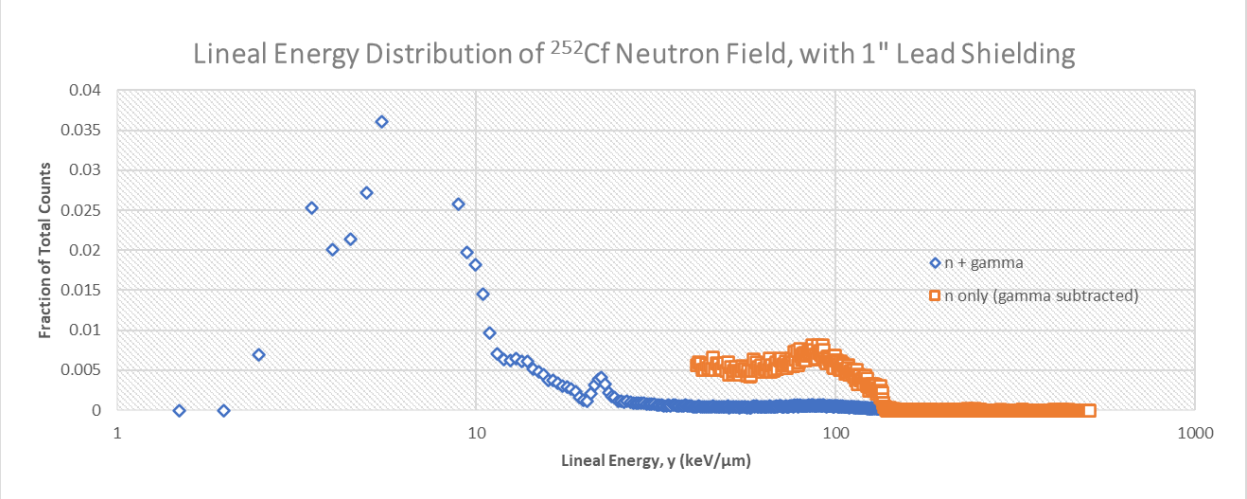

Figure 3.8 Lineal Energy Distribution for the ^{252}Cf Neutron Field with 1” Lead Shielding, 1 µm Simulated Diameter

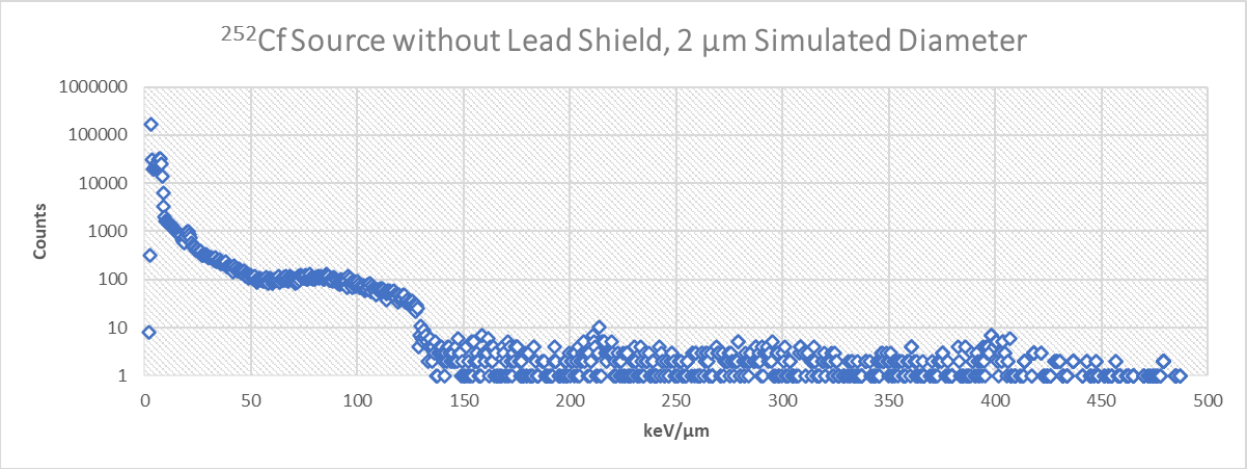

Figure 3.9 ^{252}Cf Source without Lead Shield, 2 µm Simulated Diameter

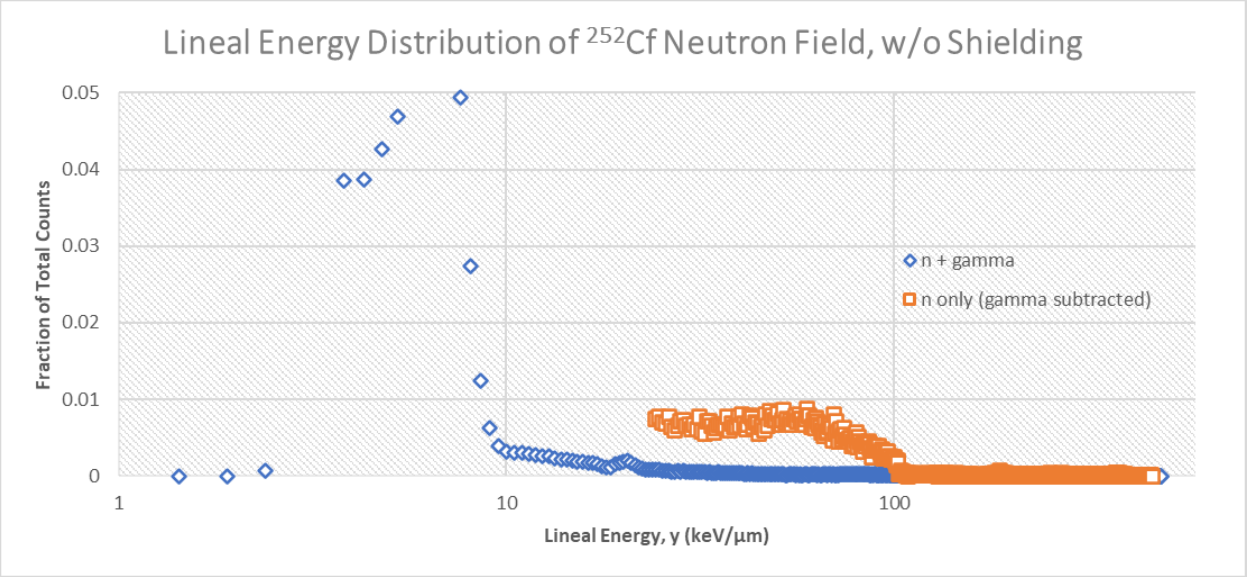

Figure 3.10 Lineal Energy Distribution for the ^{252}Cf Neutron Field without Lead Shielding, 2 µm Simulated Diameter

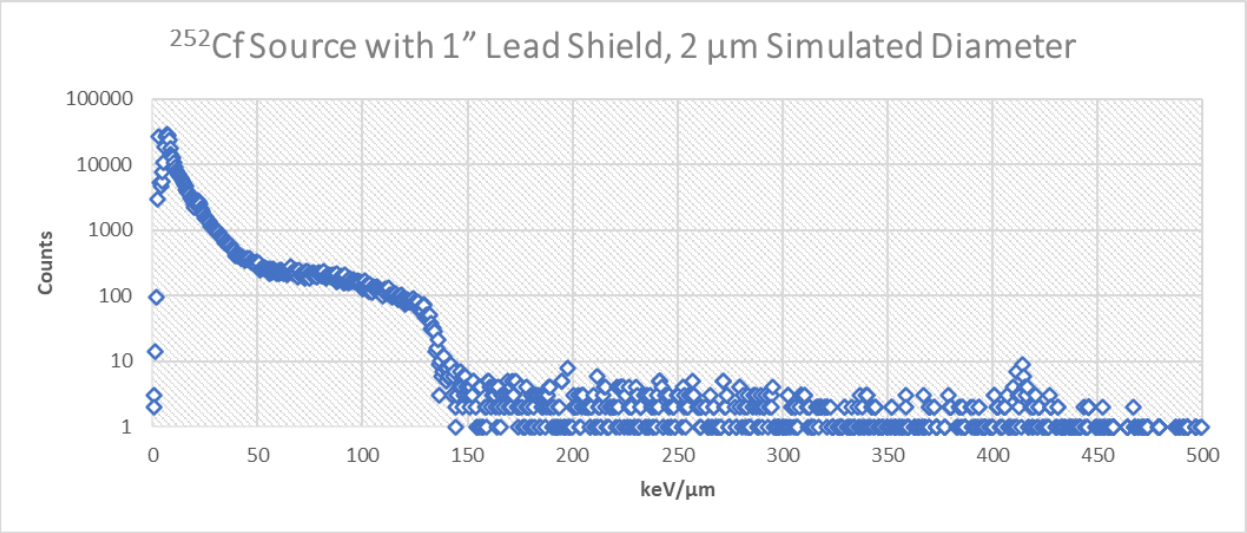

Figure 3.11 ^{252}Cf Source with 1” Lead Shield, 2 µm Simulated Diameter

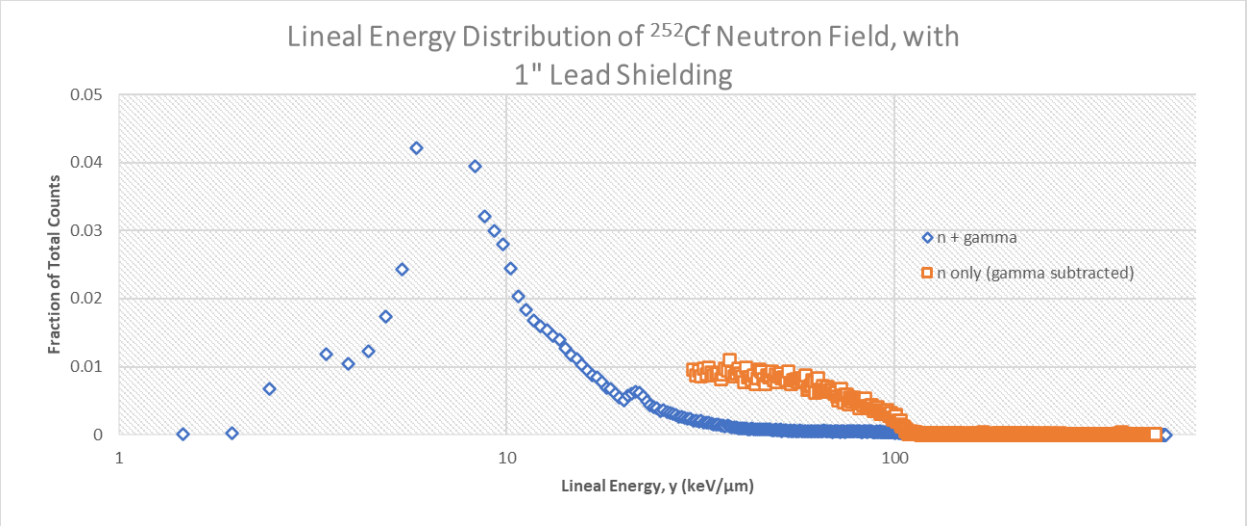

Figure 3.12 Lineal Energy Distribution for the ^{252}Cf Neutron Field with 1” Lead Shielding, 2 µm Simulated Diameter

DT Neutron Generator

The DT neutron generator was sampled at 214 cm from the source. The TEPC was placed inside a stainless steel PHCbi MCO Incubator (PHC Corporation of North America, Wood Dale, IL) to sample and quantify the exposure of tissue being irradiated inside the incubator. The DT neutron source was operated in a continuous mode, with the voltage set at 60 kV, and the current set to 1.6 mA to produce a consistent fluence of 14.1 MeV neutrons at a yield of approximately

1×10^{10} neutrons per second. Interactions with the 14.1 MeV neutrons generated from the DT generator are shown in Figure 3.13. Figure 3.14 showcases the lineal energy distribution for the DT neutron field. Sampling of the DT neutron source lasted for 2.10 hours. The spectrum shows more interactions in the lower energy regions versus higher energy regions, and is most likely due to the high-energy neutrons passing through the TE volume of the TEPC without interacting. Table 3.1 highlights the measured LET and absorbed dose from the sample event. No additional shielding was used when sampling the DT neutron source because little to no photons were emitted by the source. However, over time as the incubator is irradiated, cobalt constituents within the stainless steel wall may be activated and produce ^{60}Co that emits 1.17 and 1.33 MeV photons. The 1 µm simulated diameter was not tested with the DT neutron source.

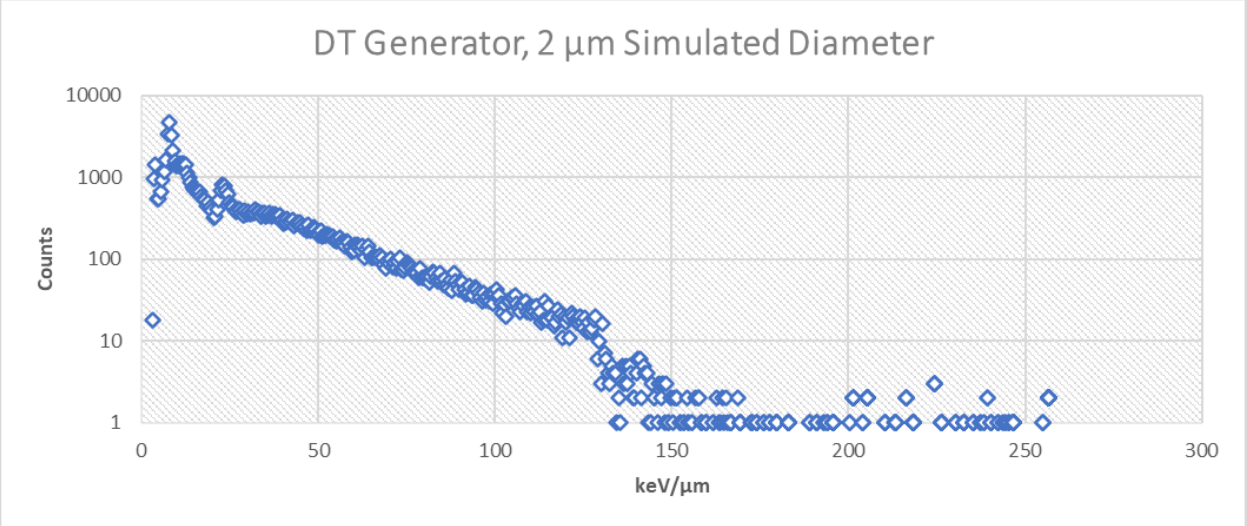

Figure 3.13 DT Generator, 2 µm Simulated Diameter

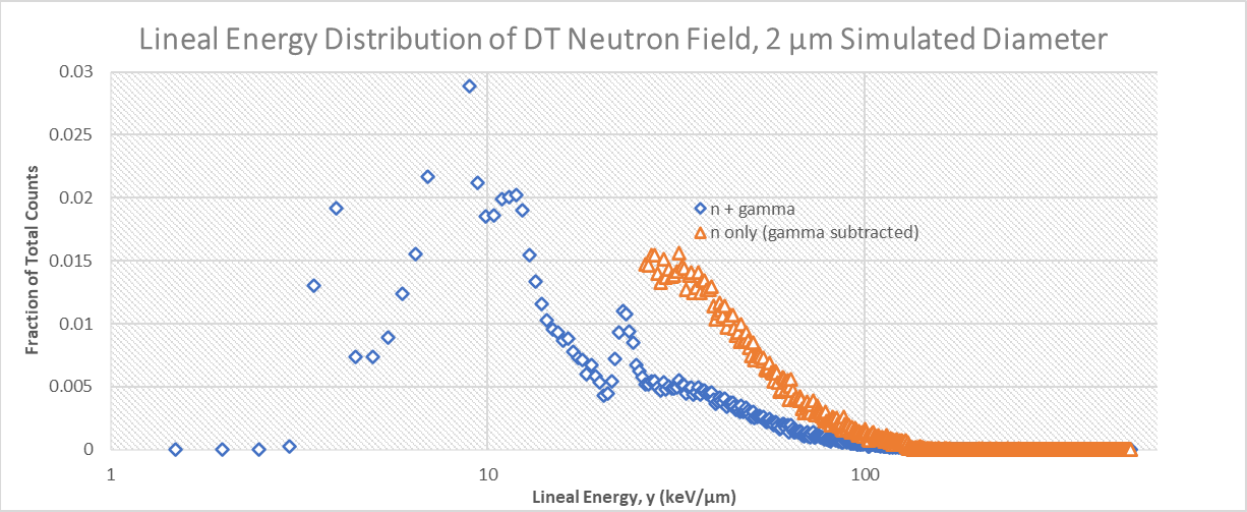

Figure 3.14 Lineal Energy Distribution for the DT Neutron Field, 2 µm Simulated Diameter

Experimental Results

The frequency-mean lineal energy ($\bar{y}_F$), dose-mean lineal energy ($\bar{y}_D$), experimental dose-average LET, and absorbed dose rate were calculated from the measurements recorded (Table 3.1 below). The theoretical external dose rate (D_E) was determined with the calculated fluence for each sample location and the neutron dose rate factor based on the average neutron energy for each source:

$$D_E = \frac{\phi}{K_n} \cdot Q \quad [\text{mGy h}^{-1}] \qquad \textbf{Equation 3.1}$$

Where: ϕ = neutron fluence at a distance from the source

K_n = neutron dose rate factor

Q = quality factor (if needed for conversion)

The data in Table 3.1 highlight unique traits for the LET and absorbed dose. Comparing the two PuBe measurements with and without lead shielding, the sample with 2" lead shielding had higher LET by 14.9%, but resulted in a lower absorbed dose rate of -34.8%. The reduction in absorbed dose rate indicates that gamma interactions contributed to over a third of the observable

dose. Comparing the PuBe sample events between 1 and 2 μm simulated diameter, the $\bar{y}_D$ and dose-average LET for the 2 μm diameter was almost the same as the 1 μm simulated diameter. The 2 μm diameter absorbed dose rate is roughly 33% greater than the 1 μm simulated diameter dose rate.

When comparing the ^{252}Cf measurements, there was a 2.78% increase in LET from shielding vs. without shielding, however, instead of seeing a lower absorbed dose rate, the dose rate increased by 66.4%. The difference in absorbed dose rate may be attributed to changes in sample geometry when measuring the ^{252}Cf source unshielded. To avoid the fixed lead barrier placed around the ^{252}Cf source, the TEPC was operated just below the lead shield 1 meter from the source, see Figure 3.15. When sampling the ^{252}Cf source below the lead shield, the source may be partially blocked/scattered by the neutron irradiator lift mechanism, reducing the amount of neutron interactions within the TEPC, and lowering the absorbed dose. In addition to testing shielding interactions, the simulated tissue diameter was compared to determine if there were any significant differences (Table 3.1). Comparing the ^{252}Cf sample events between 1 and 2 μm simulated diameter, $\bar{y}_D$ and dose-average LET for the 2 μm diameter was almost the same as the 1 μm simulated diameter. The 2 μm diameter absorbed dose rate is roughly 141% greater than the 1 μm simulated diameter dose rate. Ideally, the absorbed dose rate will increase as the simulated diameter increases, however, different factors may play a role in this difference.

Figure 3.15 ^{252}Cf Source Unshielded Sample Event

The DT generator was sampled with a 2 µm TEPC simulated diameter, resulting in a dose-average LET similar to the ^{252}Cf source. However, the absorbed dose rate measured from the DT generator was 2.85 times greater than the ^{252}Cf source with 2 µm simulated diameter and 1” lead shielding. The difference in neutron fluence between the ^{252}Cf source and the DT neutron source shows a significant increase in interactions with the TEPC. The theoretical external dose rate differed between the absorbed dose rates for all three sources. The difference between the theoretical and measured dose rates can be attributed to photon and neutron interactions measured by the TEPC. Furthermore, the theoretical dose rates were based on the average neutron energy and will not account for the array of high-energy neutrons produced by the ^{252}Cf

source. The theoretical dose rate for the DT generator was greater than the measured dose rate and may be attributed to the lack of interactions between the high energy neutrons and the TE volume.

Table 3.1 Experimental Results Based on LET-½" TEPC Measurements

Source	Live Time (h)	$\bar{y}_F$ (keV μm^{-1})	$\bar{y}_D$ (keV μm^{-1})	Dose-Average LET (keV μm^{-1})	Theoretical External Dose Rate* (mGy h^{-1})	Absorbed Dose Rate (mGy h^{-1})	Absorbed Dose (mGy)
PuBe w/2" Lead Shield, 1 µm	19.0	39	75	66	0.45	0.71	13
PuBe w/o Lead Shield, 2 µm	19.2	35	65	58		1.5	29
PuBe w/2" Lead Shield, 2 µm	19.9	47	75	67		0.94	19
^{252}Cf w/1" Lead Shield, 1 µm	22.6	14	52	46	0.04	0.16	3.7
^{252}Cf w/o Lead Shield, 2 µm	22.7	8.7	48	43		0.24	5.4
^{252}Cf w/1" Lead Shield, 2 µm	22.8	17	50	44		0.40	9.0
DT Generator, 2 µm	2.10	26	50	44	4.9	1.1	2.4

*Note: Theoretical external dose rates are based on max fluence output from the source to the detector at the distance measured, and calculated using the energy-approximate neutron dose rate factor from Table 1004(b).2. in 10 CFR 20. See Appendix B for example calculations.

Normalizing absorbed dose rate data from neutron fluence is important for accurate and meaningful radiation dose assessment. Table 3.2 identifies the normalized neutron absorbed dose rate based on each sample fluence. Neutron fluence represents the number of neutrons passing through a particular area, while absorbed dose rate measures the amount of energy deposited in a material per unit of mass. By normalizing the absorbed dose rate data, we adjust it to a standard reference condition, enabling comparisons between different measurement locations, time periods, and experimental setups. The normalized data below includes samples from shielded measurements to account for neutron interactions. The normalized values calculated show how neutrons emitted by each source contribute to the absorbed dose measured by the TEPC. Neutron energy plays a role in the amount of interactions that occur within the TEPC.

Table 3.2 Normalized Neutron Absorbed Dose Rates

Source	Distance Sampled (cm)	Sampled Neutron Fluence (n cm^{-2} sec^{-1})	Absorbed Dose Rate (mGy h^{-1})	Normalized Absorbed Dose Rate (mGy h^{-1})
PuBe w/2” Lead Shield, 1 µm	15	2.3×10^3	0.71	0.31
PuBe w/2” Lead Shield, 2 µm			0.94	0.41
^{252}Cf w/1” Lead Shield, 1 µm	100	3.2×10^2	0.16	0.51
^{252}Cf w/1” Lead Shield, 2 µm			0.40	1.2
DT Generator, 2 µm	214	1.7×10^4	1.1	0.07

Dose Equivalent Rates

Referencing the Q-L relationship from ICRP 60 (Table 2.5), the quality factor was determined by the dose-average LET values calculated. The dose-average LET used in this

experiment accounts for gamma and neutron interactions measured within the TEPC and was used to determine the source specific quality factor. The quality factor from ICRP 60 (Table 2.5) is used to calculate the dose equivalent rate from the absorbed dose rates measured in Table 3.1. The dose equivalent rates, based on ICRP 103 (Table 2.6), were calculated using the radiation weighting factor (w_R) for the sampled source and the absorbed dose rate from Table 3.1. The radiation weighting factor accounts for the average neutron energy emitted, excluding the photon emission from the sources sampled. Table 3.3 identifies the corresponding dose equivalent by using the two different conversion factors. Comparing the dose equivalent rate for the PuBe sources, the dose equivalent rates using the radiation weighting factor are roughly half those obtained by the ICRP 60 method. The dose equivalent rates for the DT neutron source are higher using ICRP 60 versus ICRP 103. However, when comparing the ^{252}Cf dose equivalent rate, the dose rate using the ICRP 103 method is larger. The difference between the quality factor and the radiation weighting factor will correlate to the difference between the methods used to calculate each value.

Table 3.3 Quality Factors (Q), Radiation Weighting Factors (w_R) and Dose Equivalent Rates

Source	Q (ICRP 60)	Dose Equivalent Rate (ICRP 60) (mSv h^{-1})	w_R (ICRP 103)	Dose Equivalent Rate (ICRP 103)* (mSv h^{-1})
PuBe w/2” Lead Shield, 1 µm	19.0	13	12.5	8.8
PuBe w/o Lead Shield, 2 µm	16.5	25		19
PuBe w/2” Lead Shield, 2 µm	19.2	18		12
^{252}Cf w/1” Lead Shield, 1 µm	12.6	2.1	17.1	2.8
^{252}Cf w/o Lead Shield, 2 µm	11.6	2.8		4.1

^{252}Cf w/1” Lead Shield, 2 μm	12.0	4.7		6.8
DT Generator	11.9	13	7.65	8.6

*Note: Dose equivalent rates using radiation weighting factors from ICRP 103 only account for the average neutron energy emitted from the source, and do not account for photon emission.

DISCUSSION

Spectrum Analysis

The interpretation of the pulse height spectrum from a TEPC is not trivial. In Figure 4.1 the pulse height distribution spectrum outlines peak characteristics of different regions (A, B, and C), where each region represents the energy deposition distributed within the TEPC based on the incident particle/photon interaction. Depositions in region A are from neutrons and/or photons that pass through an annular area corresponding to the dimensions of the plastic wall (A-150) of the TEPC. Electrons that originate in the TE wall and penetrate into the TE-sensitive volume cause events in region A. Events in region B are due to recoil protons that pass through the center of the detector or the sensitive volume of the TEPC. Large energy depositions in region C also have an annular pattern, as well as a cluster of events along a line through the detector. These events have a mean impact parameter that is near the diameter of the sensitive volume (Gersey, 2006). Therefore, when a neutron strikes the inside edge of the wall, the wall becomes ionized, and a large number of delta rays penetrate into the TE-sensitive volume and create a large pulse that resembles the passage of a high LET particle through the gas volume. In addition, neutrons may pass through the sensitive volume and strike the anode or helix wires, resulting in a burst of electrons from the wire producing a large pulse that can generate very high LET particles. The proton edge, or drop point, represents the maximum energy that a proton can deposit at the end of its range within the TE sphere. The inflection point can be used to energy calibrate the detector, however, there is uncertainty in defining the value of maximum energy deposition since the stopping power is changing rapidly when the proton nears the end of its range (Borak, 2019).

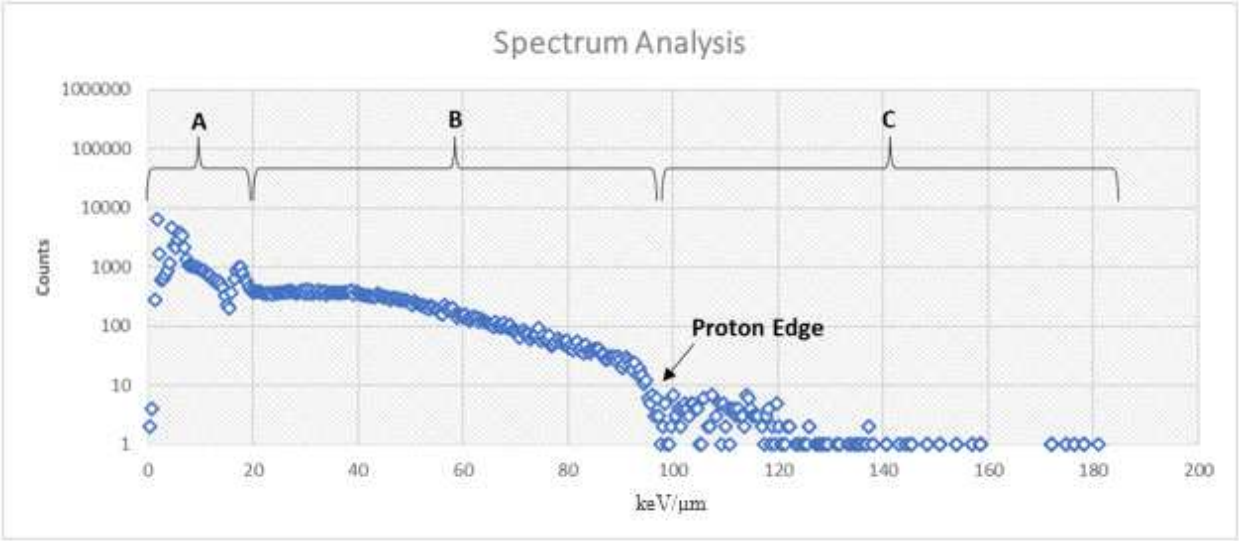

Figure 4.1 Spectrum Analysis

Disrupting Factors

An unsolved problem encountered with the TEPC is the interference of the events that dominate the low-energy region of the spectrum. Events in the low energy region can mask or skew neutron energy deposition events as seen in the figures throughout the results section. The amplifier course and fine gain were minimized, requiring high signal thresholds before the detector could record any event to ensure that the events in region A were relevant. Additionally, the electronic setup was screened using an oscilloscope to ensure any noise entering the preamplifier or shaping amplifier was kept to a minimum. Background noise was minimal to non-existent due to precautions and measurements made using the oscilloscope. To evaluate signal events in region A, various check sources emitting multiple photons and beta particles were employed. Gamma and beta sources such as ^{90}Sr, ^{137}Cs, and ^{60}Co, which possessed sufficient strength to interact with the TE wall, could generate signals reaching a few keV/µm. By analyzing the photon interactions detected from the aforementioned check sources, notable low-energy signal photons and beta events were retained within the pulse height spectrum when sampling each neutron source. The significant interactions measured in region A contributed to

determining both LET and absorbed dose calculations for this study. Lastly, a small energy peak around channel number 43 appeared in every sample run using both the ½" and 2" LET TEPC. Inquiries to the manufacturer suggest that the peak at channel 43 represents an artifact of the pole-zero cancellation or an overshoot from one of the amplifiers (Figure 4.1). The energy deposition of the peak at channel 43 in the pulse height spectrum may skew calculations but was kept as a marker between the low-energy region and the remaining spectrum.

Quality Factor Comparison

Quality factors played an important role in determining the dose-equivalent and dose-equivalent rates for neutron exposures. Changes between the methods used for ICRP 60 to ICRP 103 reflect a continuous function approach versus the step function that was used. The ICRP 103 radiation weighting factor method takes into consideration that most neutron exposures involve a range of energies instead of a monoenergetic particle, however, the use of a function to describe radiation weighting factors may not provide a better estimate of the dose-equivalent. The radiation weighting factor is decreased in the low-energy range to account for secondary photon interactions within the human body according to ICRP 103. The ICRP changes in radiation weighting factors allow for better dose characterization of neutrons at various energies based on the average neutron energy emitted by the source. Significant differences in dose-equivalent rates are observed with the PuBe source measurements where the equivalent dose rate decreased by 35.2%. The difference between the two dose equivalent rates for the PuBe source may be attributed to large energy gamma interactions (^{13}C excitation photons) within the TEPC. Meanwhile, differences in dose-equivalent rates were observed with the ^{252}Cf source (2 micron) measurements where the dose rate increased up to 48%. The difference between the two absorbed dose rates for the ^{252}Cf source may be attributed to the

change in sample geometry for the unshielded source sample event, which may have caused a reduction of neutron interactions within the TEPC. Lastly, the DT generator dose equivalent rates differ for each ICRP method due to the amount of elastic scattering events that contributed to the dose-average LET deposited within the TEPC resulting in a larger quality factor than the radiation weighting factor.

Mechanical and Human Errors

The TEPC is susceptible to both mechanical and human errors. Electronic noise can cause significant interference when collecting data and various controls must be in place to avoid false readings in data collection. Pressure is another variable that can alter the pulse height distribution and simulated diameter being tested. The pressure system allows for ± 0.3 torr to enter or exit the TEPC and the TEPC is self-calibrating, however, the detector undergoes channel shifts if pressure or temperature changes during the time of the measurement. Additionally, if the TEPC is moved or bumped during operation, significant noise will be produced or could char the anode wire. The best way to avoid this issue is to power off the detector before changing sample positions. Lastly, all computational measurements made on the pulse height distribution were done using the USX software and Excel, any errors made are most likely human mistakes in data conversion.

CONCLUSION

Overview

Space radiation is a pressing concern for astronauts, and accurately measuring radiation doses at microdosimetric volumes is essential for their safety. However, traditional dosimeters often fail to capture the true extent of damage at the microscopic level. To address this limitation, TEPCs offer a solution by accurately measuring radiation doses in microdosimetric volumes. This advanced technology not only aids in understanding potential biological effects but also characterizes mixed LET environments in space. By quantifying absorbed doses, TEPC measurements contribute to the development of effective strategies for protecting astronauts during space exploration. In this study, the simulated interactions of mixed LET radiation, including photons and neutrons, within 1-2 μm diameters of human tissue, provide valuable insights into the effects of radiation exposure on biological systems.

Measurements from different neutron sources enabled the investigation of various scenarios involving the exposure of human tissue to varying energies and quantities of photons and neutrons in space. The recorded interactions from the ^{252}Cf, PuBe, and DT neutron sources primarily illustrated how radiation deposits energy into the TE volume of the TEPC. Table 3.1 documented how the lineal energy deposited in the TEPC determined the absorbed dose and dose-average LET observed from each neutron source. Operational dose equivalents were derived from absorbed dose and LET-based quality factors, providing a comprehensive assessment for each monitored source. In contrast, dose equivalents derived from the ICRP 103 method were limited to average neutron energy, excluding photon and additional neutron contributions.

The main study was to quantify and compare TEPC dose-equivalent rates in microdosimetric volumes to determine if significant dosimetric differences exist between mixed LET environments generated by photons and neutrons. In summary, the TEPC demonstrated its ability to monitor and measure in mixed-LET environments generated by each sampled source. The TEPC successfully captured the absorbed dose produced from high-energy photon and neutron interactions depositing energy within the TE material inside. The findings from this experiment showed that mixed LET environments where both photons and neutrons interacted with the TEPC had lower LET values than neutron only exposures, and produced varying dose equivalent rates that were dependent on the source characteristics. These results revealed that the TEPC accounted for photon and neutron interactions typically overlooked in theoretical dose calculations, resulting in varying absorbed dose estimations depending on shielding, tissue density, and radiation energy present. The photons emitted by each source played a crucial role in the dose-average LET and absorbed dose outcome. Overall, the microdosimetric values obtained from the TEPC serve as a valuable reference tool for researchers studying the impact of mixed radiation fields on human tissue.

Future Studies

Further experiments, leveraging the presented research could involve additional shielding or the use of different moderating materials to test significant changes in LET and dose deposition on the detector. We expect that removing the aluminum shell of the TEPC may reduce noise contributed by delta rays produced in the outer wall. A further comparison between fluence-based measurements using a rem ball or Bonner spheres will also help quantify the efficiency of the TEPC's measurements. The TEPC can likewise provide real-time

microdosimetry for human heart tissue sampled in studies quantifying dose from high-energy neutrons with the DT neutron generator. Other microdosimetric volumes studying the effects on human tissue can be adjusted by switching to a LET-2” TEPC to quantify the absorbed dose at larger volumes (e.g., 10 μm).

REFERENCES

1. Kellerer, A. (1972). *An Algorithm for LET-Analysis.* Retrieved from: https://citeseerx.ist.psu.edu/document?repid=rep1&type=pdf&doi=edf5dc865c2b50c54e9ebbae152ab8edfcd77e90.
2. Museum of Radiation and Radioactivity. (2022). *Rossi Tissue Equivalent Proportional Counter.* Retrieved from: https://www.orau.org/health-physics-museum/collection/proportional-counters/rossi.html.
3. Borak, T.B, et al. (2019). *Design and Dosimetry of a Facility to Study Health Effects Following Exposures to Fission Neutrons at Low Dose Rates for Long Durations*. International Journal of Radiation Biology, DOI: 10.1080/09553002.2019.16888 84.
4. DT110 Neutron Generator – Adelphi Technology. (n.d.). Retrieved from: https://adelphitech.com/products/dt109-dt110.html.
5. Far West Technology, Inc. (n.d.). LET-1/2 Spherical TE Proportional Counter Data Sheet. Retrieved from: https://www.fwt.com/detector/let1_2ds.html.
6. Corporation, N. & Nuclear-Chicago Corporation. (1963). *Model NH-3 Neutron Howitzer; Operation and Maintenance Manual. Ill.*
7. Kuhne, W. et al. (2009). *Biological Effects of High-Energy Neutrons Measured In Vivo Using a Vertebrate Model.* Radiation Research Vol. 172(4). Retrieved from: https://www.ncbi.nlm.nih.gov/pmc/articles/PMC2796447/
8. Stricklin, D. et al. (2021). *Neutron Radiobiology and Dosimetry.* Radiation Research Vol. 195(5). Retrieved from: https://meridian.allenpress.com/radiation-research/article/195/5/480/461406/Neutron-Radiobiology-and-Dosimetry
9. Gersey, B. (2006). *The Response of a Spherical Tissue-Equivalent Proportional Counter to Iron Particles from 200-1000 MeV/Nucleon.* Retrieved from: https://www.researchgate.net/publication/259325821_The_response_of_a_spherical_tissue-equivalent_proportional_counter_to_iron_particles_from_200--1000_MeVnucleon.
10. Cucinotta, F. et al. (2013). *How Safe Is Safe Enough? Radiation Risk for a Human Mission to Mars.* Retrieved from: https://www.ncbi.nlm.nih.gov/pmc/articles/PMC3797711/.
11. Young, S. et al. (2008). *Understanding of the Microdosimetric Quantities Obtained by a TEPC*. Journal of Nuclear Science and Technology, Supplement 5, Pages 213-216. Retrieved from: https://www.tandfonline.com/doi/pdf/10.1080/00223131.2008.10875825?cookieSet=1.
12. Manglass, L. (2009). *Omni-Directional Sensitivity Of A Tissue-Equivalent Proportional Counter For Personal Dosimetry During Extra-Vehicular Activity On The Moon*. Department of Environmental And Radiological Health Sciences.
13. Takahashi, A. et al. (2018). *Role of High-Linear Energy Transfer Radiobiology in Space Radiation Exposure Risks*. Int J Part Ther. Summer; 5(1):151-159. doi: 10.14338/IJPT-18-00013.1. Epub 2018 Sep 21. PMID: 31773027; PMCID: PMC6871591. Retrieved from: https://www.ncbi.nlm.nih.gov/pmc/articles/PMC6871591/.
14. ICRP (2007). *The 2007 Recommendations of the International Commission on Radiological Protection*. ICRP Publication 103. Ann. ICRP 37 (2-4).
15. ICRP (1990). *Recommendations of the International Commission on Radiological Protection*. ICRP Publication 60. Ann. ICRP 21 (1-3).

16. NNDC. (n.d.). *Nuclear Decay Data in the MIRD Format.* Retrieved from: https://www.nndc.bnl.gov/nudat3/mird/.
17. NCRP. (2006). *Information Needed to Make Radiation Protection Recommendations For Space Missions Beyond Low Earth Orbit.* NCRP Publication 153.
18. Barth, U. (2017). *How Many Cells Are in Your Body? Probably More Than You Think!* Retrieved from: https://handling-solutions.eppendorf.com/cell-handling/about-cells-and-culture/detailview/news/how-many-cells-are-in-your-body-probably-more-than-you-think/.
19. NASA. (2019). *Why Space Radiation Matters*. Retrieved from: https://www.nasa.gov/analogs/nsrl/why-space-radiation-matters.
20. BEIR VII. (2006). *Health Risks from Exposure to Low Levels of Ionizing Radiation*. National Academies Press.
21. NASA. (2022). *NASA Space Flight Human-System Standard: Volume 1: Crew Health.* NASA Technical Standard 3001. Retrieved from: https://standards.nasa.gov/sites/default/files/standards/NASA/B//2022-01-05-NASA-STD-3001-Vol1-Rev-B-Final-Draft-Signature-010522.pdf.
22. Meerman, M. et al. (2021). *Myocardial Disease and Long-Distance Space Travel: Solving the Radiation Problem.* Frontiers in Cardiovascular Medicine, 8, 631985. Retrieved from: https://doi.org/10.3389/fcvm.2021.631985.
23. ICRP. (2016). *The ICRP Computational Framework for Internal Dose Assessment for Reference Adults: Specific Absorbed Fractions*. ICRP Publication 133. Ann. ICRP 45(2), 1–74. Retrieved from: https://journals.sagepub.com/doi/pdf/10.1177/ANIB_45_2.
24. ICRU. (1983). *Microdosimetry*. ICRU Report no. 36. Retrieved from: https://pubs.rsna.org/doi/10.1148/radiology.154.2.528.

APPENDIX A - DEFINITIONS

ICRP publications, such as ICRP 103, provide guidance on radiation protection. These publications outline definitions and concepts related to radiation dose quantities, radiation effects, and the principles of radiation protection. In addition, the International Commission on Radiation Units and Measurements (ICRU) develops standards and recommendations for the use of radiation in medicine and industry, including definitions of key terms and units used in radiation measurements. These definitions are listed below:

Absorbed Dose (*D*) - The fundamental dose quantity given by $D = \frac{dE}{dm}$ where *dE* is the mean energy imparted to matter of mass *dm* by ionizing radiation. The SI unit for absorbed dose is joule per kilogram (J kg^{-1}) and its special name is gray (Gy).

Becquerel (Bq) - The special name for the SI unit of activity, 1 Bq = 1 s^{-1} (2.7×10^{-11} Ci).

Bragg-Gray Cavity Theory - Bragg-Gray theory relates dose to the medium, D_{med}, to dose to the cavity fill gas, D_{gas}, via the ratio of mass collision stopping powers between the medium and gas, $\frac{D_{med}}{D_{gas}} = \frac{S_{med}}{\rho_{gas}}$

Bragg Peak - Because energy loss by Coulomb interaction is proportional to $1/v^2$, a large portion of a charged particle's energy is lost near the end of its path. This phenomenon results in a significant increase in deposited dose near the end of a charged particle's path. This increased dose deposition is known as a Bragg Peak.

Deterministic Effect - Injury in populations of cells, characterized by a threshold dose and an increase in the severity of the reaction as the dose is increased further.

Dose Equivalent (*H*) - The product of *D* and Q at a point in tissue, where *D* is the absorbed dose and Q is the quality factor for the specific radiation at this point, thus: $H = D \cdot Q$. The unit of dose equivalent is joule per kilogram (J kg^{-1}), and its special name is sievert (Sv).

Dose Limit - The value of the effective dose or the equivalent dose to individuals from planned exposure situations that shall not be exceeded.

Equivalent Dose (H_T) - The dose in a tissue or organ given by: $H_T = w_R \cdot D_T$ where D_T is the mean absorbed dose from radiation in a tissue or organ, and w_R is the radiation weighting factor. Since w_R is dimensionless, the unit for the equivalent dose is the same as for absorbed dose, J kg^{-1}, and its special name is sievert (Sv).

Fluence (ϕ) - The quotient of *dN* by *da*, where *dN* is the number of particles incident upon a small sphere of cross-sectional area da, thus: $\phi = \frac{dN}{da}$

Gray (Gy) - The special name for the SI unit of absorbed dose: 1 Gy = 1 J kg^{-1}.

Kerma (K) - The quotient of the sum of the kinetic energies, dE_{tr}, of all charged particles liberated by uncharged particles in a mass *dm* of material, and the mass dm of that material. Kerma is defined as a non-stochastic quantity and dE_{tr} is the expectation value of the sum of the kinetic energies. The unit for kerma is joule per kilogram (J kg^{-1}) and its special name is gray (Gy).

Linear Energy Transfer (L or LET) - The average linear rate of energy loss of a charged particle radiation in a medium. That is, the quotient of *dE* by *dl* where *dE* is the mean energy lost by a charged particle owing to collisions with electrons in traversing a distance *dl* in matter. The unit of L is given as keV μm^{-1} for this experiment.

Lineal Energy - The quotient of ε_i by $\bar{\imath}$, where ε_i is the energy imparted to the matter in a given volume by a single energy-deposition event i, and $\bar{\imath}$ is the mean chord length of that volume. The SI unit of lineal energy is joule per meter (J m^{-1}), often given in keV μm^{-1}.

Mass Stopping Power (S/ρ) - Stopping power is commonly presented as mass stopping power which is the ratio of stopping power to the material density.

Microdosimetry - Study of radiation interactions and energy deposition at the microscopic level within biological systems.

Quality Factor (Q(L)) - The factor characterizing the biological effectiveness of a radiation, based on the ionization density along the tracks of charged particles in tissue. Q is defined as a function of the unrestricted linear energy transfer, L_∞ (often denoted as L or LET), of charged particles in water. Q has been superseded by the radiation weighting factor in the definition of equivalent dose, but it is still used in calculating the operational dose equivalent quantities used in monitoring.

Radiation Weighting Factor (w_R) - A dimensionless factor by which the organ or tissue absorbed dose is multiplied to reflect the higher biological effectiveness of high-LET radiations compared with low-LET radiations. It is used to derive the equivalent dose from the absorbed dose averaged over a tissue or organ.

Relative Biological Effectiveness (RBE) - The ratio of a dose of a low-LET reference radiation to a dose of the radiation considered that gives an identical biological effect. RBE values vary with the dose, dose rate, and biological endpoint considered. In radiological protection, the RBE for stochastic effects at low doses is of particular interest.

Safety - The achievement of proper operating conditions, prevention of accidents, or mitigation of accident consequences.

Sievert (Sv) - The special name for the SI unit of equivalent dose, effective dose, and operational dose quantities. The unit is joule per kilogram ($J\ kg^{-1}$).

Source - An entity for which radiological protection can be optimized as an integral whole. Sources of radiation, such as radiation generators and sealed radioactive materials, and, more generally, the cause of exposure to radiation or to radionuclides.

Stochastic Effects - Malignant disease and heritable effects for which the probability of an effect occurring, but not its severity, is regarded as a function of dose without threshold.

Stopping Power (S) - The energy loss by charged particles per unit path length of a material.

Townsend Avalanche - A cascade reaction involving electrons in a region with a sufficiently high electric field. Incoming radiation ionizes one of the atoms or molecules in the medium. The positive ion drifts towards the cathode, while the freed electron drifts towards the anode of the chamber. It accelerates in the electric field, gaining sufficient energy such that it frees another electron upon collision with another atom/molecule of the medium.

APPENDIX B - EXAMPLE CALCULATIONS

Density of TE Gas at 1 µm = $\rho_{gas} = \frac{\rho_t \cdot d_t}{d_{gas}} =$

$$\frac{0.0001 \text{ cm} \cdot 1.04 \text{ g cm}^{-3}}{1.27 \text{ cm}} = 0.0000819 \text{ g cm}^{-3}$$

TEPC Gas Pressure for 1 µm Simulated Diameter = $P_{gas} = \frac{\rho_{gas}}{MW} \cdot R \cdot T =$

$$\frac{0.0000819 \text{ g cm}^{-3}}{43.1 \text{ g mol}^{-1}} \cdot 62{,}364 \text{ cm}^3 \text{ torr mol}^{-1} \text{ K}^{-1} \cdot 293 \text{ K} = 34.7 \text{ torr}$$

Theoretical External Dose Rate for PuBe (5 MeV) at 15 cm = $\frac{\phi}{K_n} \cdot Q =$

$$\frac{2{,}298.9 \text{ n cm}^{-2} \text{ sec}^{-1}}{23 \times 10^6 \text{ n cm}^{-2} \text{ rem}^{-1}} \cdot \frac{3{,}600 \text{ sec}}{1 \text{ h}} \cdot \frac{0.125 \text{ rad}}{1 \text{ rem}} \cdot \frac{1 \text{ Gy}}{100 \text{ rad}} \cdot \frac{1{,}000 \text{ mGy}}{1 \text{ Gy}} = 0.450 \text{ mGy h}^{-1}$$

PuBe Neutron Fluence (n cm^{-2} sec^{-1}) at 15 cm = $\frac{N}{4 \cdot \pi \cdot x^2} =$

$$\frac{6.5 \times 10^6 \text{ n } sec^{-1}}{4 \cdot \pi \cdot (15 \text{ cm})^2} = 2{,}298.9 \text{ n cm}^{-2} \text{ sec}^{-1}$$

Normalized Neutron Absorbed Dose Rate for PuBe, 1 µm = $D_N = \frac{D \cdot 1{,}000}{\phi} =$

$$\frac{0.705 \text{ mGy h}^{-1} \cdot 1{,}000}{2{,}298.9} = 0.31 \text{ mGy h}^{-1}$$

Dose Equivalent Rate (ICRP 60) (mSv h^{-1}) for PuBe with 1" Lead Shield, 1 µm = $H = D \cdot Q =$

$$0.705 \text{ mGy h}^{-1} \cdot 19 = 13.4 \text{ mSv h}^{-1}$$